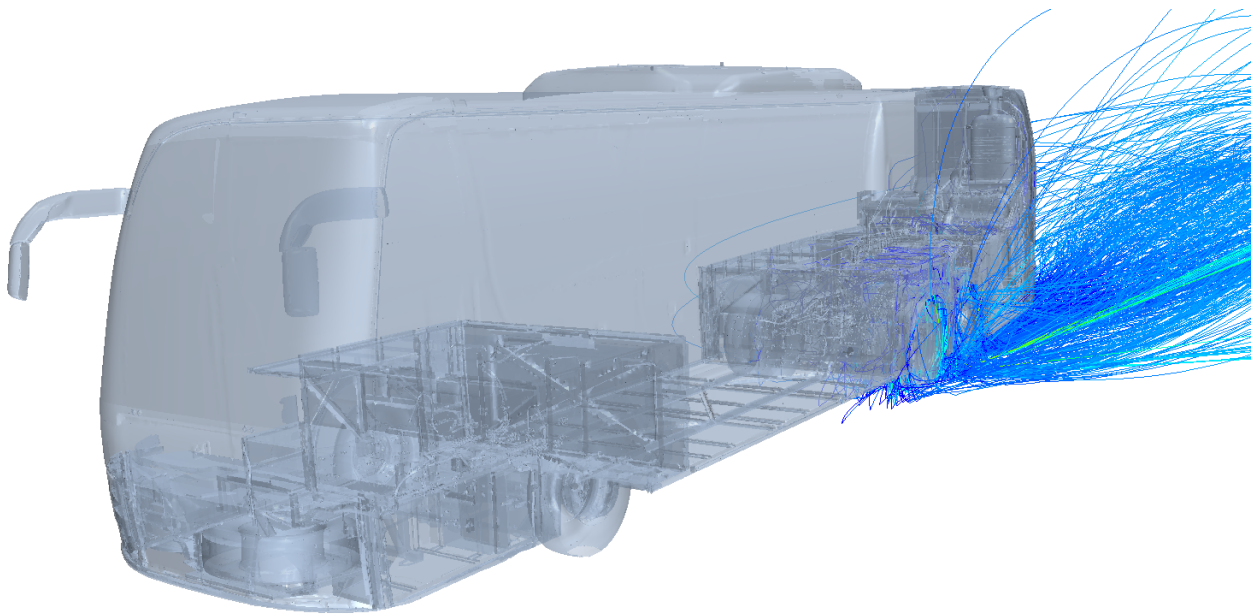




CHALMERS



Numerical simulation of particle soiling in the engine compartment of a bus

Master's thesis in Engineering Mathematics and Computational Science

SIMON LINDBERG

MASTER'S THESIS IN ENGINEERING MATHEMATICS AND COMPUTATIONAL SCIENCE

Numerical simulation of particle soiling in the engine compartment of a bus

SIMON LINDBERG

Department of Applied Mechanics
Division of Fluid Mechanics
CHALMERS UNIVERSITY OF TECHNOLOGY
Göteborg, Sweden 2015

Numerical simulation of particle soiling in the engine compartment of a bus
SIMON LINDBERG

© SIMON LINDBERG, 2015

Master's thesis 2015:30
ISSN 1652-8557
Department of Applied Mechanics
Division of Fluid Mechanics
Chalmers University of Technology
SE-412 96 Göteborg
Sweden
Telephone: +46 (0)31-772 1000

Cover:
Particles around a Volvo 9700 bus, released from the wheels and colored by velocity.

Chalmers Reproservice
Göteborg, Sweden 2015

Numerical simulation of particle soiling in the engine compartment of a bus
Master's thesis in Engineering Mathematics and Computational Science
SIMON LINDBERG
Department of Applied Mechanics
Division of Fluid Mechanics
Chalmers University of Technology

ABSTRACT

The location of the air intake of a bus creates challenges from a soiling perspective. The proximity to the rear wheels pulls up dirt from the road. Compared to a commercial truck, with the fan placement in the front of the vehicle the air intake of a bus can't rely on ram air pressure to get the sufficient cooling air mass flow. The fan must always operate on high effect when the bus is driving and thus pulls in dirt. An understanding of the flow of the dirt in the engine is necessary for a possibility to prevent it from soiling the engine compartment. As physical evaluation of the dirt flow is very complicated a numerical method has been developed in the present work. The computational fluid dynamics software STAR-CCM+ was used to simulate the airflow and the particles released in front, under and from the rear wheels on the same side as the air intake of the bus. Steady Lagrangian particle tracking was used to simulate the particle movement. The method developed can be used to get a basic understanding of where the dirt particles enter the engine compartment. The method is demonstrated for the flow around a fully detailed Volvo bus which includes cooling package and engine compartment. The demonstration shows that the method can be used to analyse particle tracks, the size of particles enters the engine compartment, the impact of different grilles on the particle intake, the difference in the particle intake depending on the amount of air entering the engine compartment, the effect of the bus speed and the difference when changing the geometry around the engine compartment on the number of particles entering the bus engine compartment.

Keywords: cfd, soiling, engine compartment, lagrangian, steady, MRF, porous media, dirt

PREFACE

This thesis was carried out in the spring of 2015 at technical analysis, ÅF Industry, in collaboration with the Engine compartment & Supporting System, CD74150 group at Volvo Buses with the goal of developing a method for modelling the soiling of a bus engine compartment.

ACKNOWLEDGEMENTS

I would like to thank everybody who have made this thesis possible. A great thanks to technical analysis at ÅF for invaluable help and the time spent helping me. A special thanks to my supervisor Jan Östh for all the time in discussing ideas and making sure the report is understandable and to Mark Saukkonen for making the project happen.

A big thanks also goes to Volvo Buses and to Dalibor Cuturic for the time and energy given to support the project with ideas and great help and to Linda Frank for the possibility to work with this project.

At Chalmers I would like to thank my examiner Sinisa Krajnovic, Srdjan Sasic for helping me understand the behavior of particles and Henrik Ström for sitting down and discussing the project.

A thanks also goes to Chrisofer Wanner at CD-Adapco Sweden for providing a licence for the CFD software STAR-CCM+ and to BETA CAE systems for providing a licence for the software ANSA. The support for STAR-CCM+ from Gabriel Amine-Eddine at CD-Adapco was also appreciated.

NOMENCLATURE

SYMBOLS

| Symbol | Description |
|---------------|--|
| μ | Dynamic viscosity |
| ν | Kinematic viscosity |
| ρ | Density |
| τ_{ij} | Viscous stress tensor |
| C_d | Drag Coefficient |
| C_p | Pressure Coefficient |
| k | Turbulent kinetic energy |
| ε | Dissipation |
| p | Pressure |
| p_{abs} | Absolute pressure |
| Re | Reynolds number |
| u_i | Velocity in Einstein notation |
| u_η | Kolmogorov scale velocity |
| l_η | Kolmogorov scale length |
| τ_η | Kolmogorov scale time |
| L_{int} | Integral length scale |
| x_i | Position |
| f_i | Body force |
| δ_{ij} | Kronecker delta |
| s_{ij} | Strain rate tensor |
| e | Energy |
| F_i | Force |
| T_i | Torque |
| ω | Rotational velocity |
| e_t | Coefficient of restitution in tangential direction |
| e_n | Coefficient of restitution in normal direction |

ACRONYMS

| | |
|------|---------------------------------|
| CFD | Computational Fluid Dynamics |
| DNS | Direct Numerical Simulation |
| RANS | Reynolds Averaged Navier Stokes |
| CAC | Charge air cooler |
| MRF | Multiple Reference Frame |
| CAD | Computer Aided Design |

CONTENTS

| | |
|---|------------|
| Abstract | i |
| Preface | iii |
| Acknowledgements | iii |
| Nomenclature | v |
| Contents | vii |
| 1 Introduction | 1 |
| 1.1 Background | 1 |
| 1.2 Flow around a bus | 2 |
| 1.3 Purpose | 2 |
| 1.4 Limitations | 2 |
| 1.5 Outline | 2 |
| 2 Theory and modelling | 3 |
| 2.1 Turbulent flow | 3 |
| 2.1.1 Governing equations | 3 |
| 2.1.2 Averaging and filtering of turbulent flow | 4 |
| 2.1.3 Realizable $k - \varepsilon$ model | 4 |
| 2.2 Particle flow | 5 |
| 2.2.1 Governing equations for the particles | 5 |
| 2.2.2 Steady Particle Tracking | 6 |
| 2.3 Forces on particles | 6 |
| 2.3.1 Drag models | 6 |
| 2.3.2 Turbulent Dispersion | 7 |
| 2.4 Particle-Wall interactions | 7 |
| 2.4.1 Linear spring collision model | 7 |
| 2.4.2 Coefficient of restitution | 8 |
| 2.4.3 Adhesion | 8 |
| 2.5 Cooling package | 8 |
| 2.5.1 Heat exchanger modelling | 9 |
| 2.5.2 Modelling particles in the heat exchangers | 10 |
| 2.6 Modelling rotating objects | 10 |
| 2.6.1 Modelling Multiple Reference Frame | 10 |
| 2.7 Volume meshing | 11 |
| 2.7.1 Surface wrapping | 11 |
| 2.7.2 The mesh | 11 |
| 3 Method | 13 |
| 3.1 Softwares | 13 |
| 3.1.1 ANSA | 13 |
| 3.1.2 STAR-CCM+ | 13 |
| 3.2 Mesh Generation | 13 |
| 3.2.1 Geometry Preparation | 13 |
| 3.2.2 Surface Wrapping | 14 |
| 3.2.3 The Volume mesh | 14 |
| 3.3 Setting up multiple reference frames | 14 |
| 3.3.1 Setting up the multiple reference frames at the fan | 14 |
| 3.3.2 Turbulence model selection | 14 |
| 3.4 Particle Injectors and Lagrangian solver settings | 15 |
| 3.4.1 The dust | 15 |

| | | |
|----------|--|-----------|
| 3.4.2 | Lagrangian solver settings | 15 |
| 3.5 | Solver settings | 15 |
| 3.6 | Case A | 16 |
| 3.6.1 | Different grilles | 17 |
| 3.6.2 | The mesh and settings for Case A | 17 |
| 3.6.3 | Initial and boundary conditions | 17 |
| 3.6.4 | Particle injector | 18 |
| 3.7 | Case B | 18 |
| 3.7.1 | Mesh for Case B | 18 |
| 3.7.2 | Setting up the multiple reference frames at the wheels | 18 |
| 3.7.3 | Particle Injectors and settings | 20 |
| 3.7.4 | Initial and boundary conditions | 20 |
| 3.7.5 | Calculating the path of the particles | 21 |
| 4 | Results | 22 |
| 4.1 | Case A | 22 |
| 4.2 | Case B | 25 |
| 5 | Discussion | 30 |
| 5.1 | Case A | 30 |
| 5.1.1 | Particle diameter through the grille | 30 |
| 5.1.2 | The cooling package | 30 |
| 5.2 | Case B | 30 |
| 5.2.1 | Entering and exiting the engine compartment | 31 |
| 5.2.2 | Particles under the wheels | 31 |
| 5.3 | Limitations | 31 |
| 5.4 | Computational demands | 31 |
| 5.4.1 | Adding extra models | 32 |
| 5.4.2 | Particle tracks | 32 |
| 5.5 | Use of method | 32 |
| 5.6 | Proposed future studies | 32 |
| 6 | Conclusions | 33 |
| | References | 34 |
| A | Appendix | 36 |
| A.1 | The influence of rotation of particles | 36 |
| A.2 | Results from the rotation of particles | 36 |

1 Introduction

In this section the background to the thesis will be described, some specifics about the flow around the bus will be explained and the purpose, limitations and the outline of the thesis will be explained.

1.1 Background

Deposition of dirt is a problem in many engineering applications. The phenomena of particulate fouling is widely studied to further understand the soiling and even clogging of heat exchangers and other equipments [1]. The soiling significantly reduces the performance of heat exchangers [2] and the extra resistance and reduced heat transfer capabilities can increase the fan power consumption by 100% to maintain cooling abilities in some applications [3].

In buses, the usual location of the engine at the back of the vehicle increases the dirt deposits in the engine compartment. The dirt can enter from several entrances, the covers under the bus are not fully sealed, the air-intake to the cooling package and the opening at the back of the bus. The cooling package is usually located next to the rear wheel where road dirt from the wheel can be sucked in through the cooling package. The dirt can damage some of the more sensitive parts in the engine compartment and needs to be removed when engine service is conducted. The dirt particles entering can have many sources, material from unpaved road or construction sites, brake or tire wear, vehicle exhaust and sediment of ambient particulate matter [4]. In a study [4] analyzing particles less than $840\mu\text{m}$ it was shown that particles greater than $150\mu\text{m}$ made up a large portion of the mass fraction of the dirt. The knowledge of where the particle enters the engine compartment and what range of sizes that can enter is not fully understood and to better understand the soiling process a computational model can be utilized. Soiling has been studied before and it is usually the splashing and soiling of the doors and back of the vehicle that has been studied, for example see Gaylard 2011 where a simulation using Lattice-Boltzmann was performed to study the soiling of a car [5].

Figure 1.1 shows the grille of the bus with some wet dirt, where it can be seen that some of the dirt dirty water has hit the grille and then flowed down below the grille.



Figure 1.1: *Dirt on the grille. Image courtesy of Volvo Bus.*

1.2 Flow around a bus

The shape of a bus is usually a rectangular body with rounded edges, as can be seen on the Volvo 9500 bus in Figure 1.2. The flat front area and the relatively sharp edges on the back of the back creates a high pressure difference on the front and the back of the bus. The difference in the pressure is a large portion of the drag of the bus. The rounding on the bus has a large influence on the drag as it reduces the separation [6]. A typical value of the drag coefficient of a coach, a bus made for intercity travels, is about 0.6 but lower values are not uncommon [7]. Another important feature of the flow around the bus is the flow in and around the the wheel



Figure 1.2: *Volvo 9500 bus. Image courtesy of Volvo Bus*

house. On a car, which is more streamlined and smaller than a bus, the wheels and wheel houses account for some 25% of the total drag coefficient [8]. The flow in the wheel house is highly chaotic as the wheel is rotating and contributes to unsteady flow on the side of the bus where the engine air intake is located [9]. The particles from the wheel house can even reach higher than the wheel as they exits the wheel house [5]. The fan on a bus must run at higher speeds than fans of equivalent engines on trucks due to the location at the side of the bus. A fan in the front of the vehicle, as on passenger cars and commercial trucks, allows the ram air to be pushed inside the engine, decreasing the need of a fan at higher vehicle speed [10].

1.3 Purpose

The purpose of this thesis is to study and if possible develop a model for investigation of the particle flow into a bus engine compartment using numerical methods. A focus on the thesis will be on the cooling package as it is the most complex particle inlet to the engine compartment and the flow through the heat exchangers and the fan will be studied thoroughly.

1.4 Limitations

The project time is limited to 20 weeks. Computational processing time is limited and only steady state model will be conducted. Only dry particles will be examined in a Euler-Lagrangian framework.

1.5 Outline

The thesis will first present the theory regarding the different physical models that will be important for the project. After the theory the method chapter will explain how the project was conducted and what models in the commercial software STAR-CCM+ that was chosen for the project. The result from the different cases will be presented following the method. A discussion will be conducted on the results that later will be concluded in the conclusion. A short suggestion of possible future work will finish the thesis.

2 Theory and modelling

This section presents the theory necessary for the for the general understanding of the thesis. In section 2.1 the theory governing the fluid phase is described, in sections 2.2 to 2.4 the theory governing the particles and the interaction with the fluid and walls is described. The cooling package and the modelling of the cooling package is described in sections 2.5 and 2.6.1. Meshing is briefly described in section 2.7.

2.1 Turbulent flow

Turbulence is a property of fluid flows characterized by three-dimensional randomness and apparent chaotic behavior. Most flows that are interesting from an engineers perspective, such as flows around vehicles, the flow in air condition systems or atmospheric flows are all immensely influenced by turbulence [11]. Turbulence is both space and time dependent and the smallest scales, called the Kolmogorov microscales, where its length scale often is less than a millimeter and is defined, for the velocity, length and time scale respectively, as

$$u_\eta = (\nu\varepsilon)^{\frac{1}{4}}, \quad l_\eta = \left(\frac{\nu^3}{\varepsilon}\right)^{\frac{1}{4}}, \quad \tau_\eta = \left(\frac{\nu}{\varepsilon}\right)^{\frac{1}{2}}. \quad (2.1)$$

Where ν is the dynamic viscosity and ε is the turbulent dissipation [12]. On the other end of the spectrum is the integral scales, which is the scales of the largest eddies in a flow. The integral length scale for a point x_i in the direction of \hat{x}_i is defined as:

$$L_{int}(x_i) = \int_0^\infty \frac{\overline{u'_i(x_i)u'_i(x_i + \hat{x}_i)}}{\left(\overline{u_i(x_i)^{\prime 2}}\right)^{\frac{1}{2}} \left(\overline{u_i(x_i + \hat{x}_i)^{\prime 2}}\right)^{\frac{1}{2}}} d\hat{x}_i, \quad (2.2)$$

where u_i is the velocity in the i -th direction and x_i is a position [12].

2.1.1 Governing equations

The governing equations to describe a Newtonian fluid is the continuity equation (2.3), the momentum equation (2.4) and the energy equation (2.7). The continuity equation is an unsteady, three dimensional mass conservation equation for a compressible fluid per fluid element [13],

$$\frac{\partial \rho}{\partial t} + \frac{\partial}{\partial x_i}(\rho u_i) = 0. \quad (2.3)$$

Where ρ is the density of the fluid element. The momentum equation is derived from Newton's second law and states that the rate of increase of momentum on the fluid element is equal to the sum of forces on the same element. It is written as follows [13]:

$$\frac{\partial}{\partial t}(\rho u_i) + \frac{\partial}{\partial x_j}(\rho u_i u_j) = -\frac{\partial p}{\partial x_i} + \frac{\partial \tau_{ij}}{\partial x_j} + \rho f_i. \quad (2.4)$$

The last term, ρf_i , is body forces such as gravity. The viscous stresstensor, τ_{ij} , that acts on the fluid element is defined as [12]

$$\tau_{ij} = 2\mu s_{ij} - \frac{2}{3}\mu s_{kk}\delta_{ij}, \quad (2.5)$$

where δ_{ij} is the Kronecker delta and s_{ij} is the strain rate tensor defined as

$$s_{ij} = \frac{1}{2} \left(\frac{\partial u_i}{\partial x_j} + \frac{\partial u_j}{\partial x_i} \right). \quad (2.6)$$

The energy equation is derived from the first law of thermodynamics which says that the rate of increase of energy equals the added heat and work done on the fluid particle. The equation can be written as follows [13]

$$\frac{\partial}{\partial t}(\rho e) + \frac{\partial}{\partial x_i}(\rho e u_i) = -\frac{\partial}{\partial x_i}(p u_i) + \frac{\partial}{\partial x_i}(\tau_{ij} u_j) + \frac{\partial q_i}{\partial x_i} + \rho u_i f_i + S_e, \quad (2.7)$$

here S_e is the energy source term and q is the heat flux.

The fluids density is modelled using the ideal gas law which is formulated as [14]

$$\rho = \frac{p_{abs}}{RT}, \quad (2.8)$$

where ρ is the fluid density, p_{abs} is the absolute pressure, T is the temperature and R is the specific gas constant.

The flow is calculated using a Eulerian perspective, where a control volume in space is monitored and the velocity of the fluid flowing through the point is calculated.

2.1.2 Averaging and filtering of turbulent flow

Due to the the small scales and random behavior of turbulent flow simplifications are usually done to lessen the computational need. For very small cases with simple geometry it is possible to calculate the properties of the flow with Direct Numerical Simulations (DNS) which solves the governing equation directly without modelling. But as the scales for the turbulence decreases as the flow gets faster and more complicated the computational need for DNS fast grows beyond feasible. Therefore different kinds of averaging is performed where the most common is averaging in time and/or in space.

Reynolds averaging

A common way of averaging is the Reynolds averaging. The method is to split the variables in a time averaged part, and one fluctuating part as is shown here for the velocity and the pressure [13]:

$$u_i = \bar{u}_i + u'_i, \quad (2.9)$$

$$p = \bar{p} + p'. \quad (2.10)$$

Here the mean variables are defined as:

$$\bar{u}_i = \frac{1}{\Delta t} \int_0^{\Delta t} u_i(t) dt, \quad (2.11)$$

where Δt in theory should approach infinity but in practice is larger then the largest time scales of the flow, the integral time scale which can be calculated similar to Eq. (2.2). The fluctuating properties time average is by definition zero:

$$\overline{u'_i} = \frac{1}{\Delta t} \int_0^{\Delta t} u'_i dt = 0. \quad (2.12)$$

Using Reynolds averaging on the governing equations, Eq. (2.3) and (2.4) the Reynold averaged Navier Stokes equations (the RANS equations) is written as follows [12]

$$\frac{\partial \bar{u}_i}{\partial x_i} = 0, \quad (2.13)$$

$$\rho \frac{\partial \bar{u}_i \bar{u}_j}{\partial x_j} = -\frac{\partial \bar{p}}{\partial x_i} + \frac{\partial}{\partial x_j} \left(\mu \frac{\partial \bar{u}_i}{\partial x_j} - \rho \overline{u'_i u'_j} \right). \quad (2.14)$$

Where the new term, $\overline{\rho u'_i u'_j}$ is called the Reynold stress tensor.

2.1.3 Realizable $k - \varepsilon$ model

The $k - \varepsilon$ -model is one of the most widely used models in engineering simulations of fluid flow. It is a Reynolds averaged model that solves the governing RANS equations, Eqs. (2.13) and (2.14) and two model equation for the unresolved kinetic energy, k , and one for the unresolved dissipation, ε . This model has been shown to perform well for boundary layer flows but poorly for certain other kind of flows governed by separation and/or high mean shear rate [12]. The transport equations for the model variables k and ε are as follows below:

$$\frac{\partial \varepsilon}{\partial t} + \bar{u}_j \frac{\partial \varepsilon}{\partial x_j} = \frac{\partial}{\partial x_j} \left(\frac{\nu_t}{\sigma_\varepsilon} \frac{\partial \varepsilon}{\partial x_j} \right) + c_1 S \varepsilon - c_2 \frac{\varepsilon^2}{k + \sqrt{\nu \varepsilon}}, \quad (2.15)$$

$$\frac{\partial k}{\partial t} + \bar{u}_j \frac{\partial k}{\partial x_j} = \frac{\partial}{\partial x_j} \left(\frac{\nu_t}{\sigma_k} \frac{\partial k}{\partial x_j} \right) - \bar{u}_i \bar{u}_j \frac{\partial u_i}{\partial x_j} - \varepsilon. \quad (2.16)$$

Where $S = \sqrt{2S_{ij}S_{ij}}$ is the mean strain rate, ν_t are the turbulent viscosity, $\sigma_\varepsilon, \sigma_k, c_1, c_2$ is constants that will be defined later and

$$\bar{u}_i \bar{u}_j = \frac{2}{3} k \delta_{ij} + \nu_t \left(\frac{\partial \bar{u}_i}{\partial x_j} - \frac{\partial \bar{u}_j}{\partial x_i} \right) \quad (2.17)$$

where

$$\nu_t = c_\mu \frac{k^2}{\varepsilon}. \quad (2.18)$$

In the standard $k - \varepsilon$ model c_μ is a constant which can make the normal stresses negative and violate the Schwartz inequality for the shear stresses when the mean strain rate grows large [15]. This is not possible for a physical flow and the model is therefore said to be non-realizable in these conditions. To improve the poor performance of the standard $k - \varepsilon$, Shih et al. proposed an improved version of the $k - \varepsilon$ model, called the Realizable $k - \varepsilon$ model [15]. A new constant c_μ is proposed in the model which depends on the strain rate as

$$c_\mu = \frac{1}{A_0 + A_s U^{(*)} \frac{k}{\varepsilon}}. \quad (2.19)$$

The values of the constants used in the present work for the model are [14]:

$$\sigma_\varepsilon = 1.2 \quad \sigma_k = 1.0 \quad c_2 = 1.9 \quad A_0 = 4.0 \quad U^{(*)} = \sqrt{S_{ij}S_{ij} - W_{ij}W_{ij}}, \quad (2.20)$$

and the values of the coefficients are [14]:

$$c_1 = \max(0.43, \frac{\eta}{5 + \eta}) \quad \text{where} \quad \eta = \frac{Sk}{\varepsilon} \quad (2.21)$$

$$A_s = \sqrt{6} \cos \phi \quad \text{where} \quad \phi = \frac{1}{3} \arccos(\sqrt{6}W) \quad \text{and} \quad \text{where} \quad W = \frac{S_{ij}S_{jk}S_{ki}}{(S_{ij}S_{ij})^{\frac{3}{2}}} \quad (2.22)$$

2.2 Particle flow

The particles are modelled in a Lagrangian framework. A Lagrangian perspective is a framework where the particle or point is followed while in an Eulerian a point is chosen and the properties of particles flowing through the point is monitored. The Lagrangian framework is more suitable for a few particles while the Eulerian is more suitable for the fluid continua.

2.2.1 Governing equations for the particles

The movement of particles is simulated using Newton's second law,

$$ma_i = \sum_k F_{i,k}. \quad (2.23)$$

If the rotation is modelled the torque balance follows [14]:

$$\frac{d}{dt} L_i = \frac{d}{dt} I_i \omega_p = \sum_{\text{neighbor particles}} T_{i,\text{contact}} + \sum_{\text{neighbor boundaries}} T_{i,\text{contact}} \quad (2.24)$$

Where L_i is the particle angular momentum, I_i is the particle moment of inertia and ω_p angular velocity for the particle. The contact torque, $T_{i,\text{contact}}$, is defined as

$$T_{i,\text{contact}} = r_{i,c} \times F_{i,c} - \mu_r |r_{i,c}| |F_{i,c}| \frac{\omega_c}{|\omega_c|} \quad (2.25)$$

where $r_{i,c}$ is a vector from the particle center of gravity to the contact point. $F_{i,c}$ is the contact force acting on the particle and μ_r is the coefficient of rolling friction.

Particles and parcels

All governing equations and forces governing the particles are defined on particles. But usually CFD software use parcels. A parcel is a group of particles with the same properties as a single particle (diameter, density etc.). In STAR-CCM+ the mass of a parcel is always the same so the number of particles in a parcel varies largely with the diameter [14].

2.2.2 Steady Particle Tracking

It can be seen in Section 2.2.1 that the Lagrangian particle tracking is a time dependent method. In STAR-CCM+ it is possible to track particles steady. The steady method still depends on time marching but does the time marching after each steady iteration where the time step control is defined using the Courant number according to [14]:

$$\frac{Co_{min}\Delta x}{\max(|u_i|, |u_{i,p}|)} \leq \delta t_p \leq \frac{Co_{max}\Delta x}{\max(|u_i|, |u_{i,p}|)}, \quad (2.26)$$

where the $\max(|u_i|, |u_{i,p}|)$ is the maximum of either the fluid or the particle velocity, Δx is the cell length and Co_{max} and Co_{min} the max and min Courant number defined in the solver.

2.3 Forces on particles

There exist many different types of forces that act on the particles including the drag force, the added mass force, the history (Basset) force, lift (Magnus and Saffman) forces and turbulent dispersion [16]. The most relevant forces for the thesis will be presented below.

2.3.1 Drag models

There are two types of drag models that can be applied. One that has its source from the difference in velocities between the particle and fluid and one that has its source from the rotational difference of the particle and fluid.

Drag force

In Star-CCM+ the drag force is modelled using the Schiller-Naumann model defined as [14]

$$C_d = \begin{cases} \frac{24}{Re_d}(1 + 0.15Re_d^{0.687}) & 0 < Re_d \leq 1000 \\ 0.44 & Re_d > 1000, \end{cases} \quad (2.27)$$

Where Re_d is the particle Reynolds number defined as

$$Re_d = \frac{\rho_c |u_{i,r}| l_d}{\mu_c}. \quad (2.28)$$

Where the subscripts d and c stands for the dispersed phase (the particles) and continuous phase respectively. The subscript r stands for a relative velocity which is the difference of the velocity between the phases. ρ is the density, the l_d is a characteristic length, here the diameter and the μ is the dynamic viscosity. There are plenty other drag models that is suitable for different kind of flow and geometries of particles [17].

Drag torque

When the particle is rotating a torque drag is applied on the particle. The drag torque is due to the difference in the rotational velocities between the particle and the fluid. The model in STAR-CCM+ is by Sommerfeld and is defined as [14]

$$T_{i,drag} = \frac{\rho}{2} \left(\frac{D}{2} \right)^5 C_R |\Omega_i| \Omega_i, \quad (2.29)$$

where ρ is the particle density, D the particle diameter, C_R the rotational drag coefficient and the relative angular velocity of the particle to the fluid, Ω_i , is defined as

$$\Omega_i = \frac{1}{2} \nabla \times u_i - \omega_{i,p}, \quad (2.30)$$

where u_i is the fluid velocity. The rotational drag coefficient is defined as

$$C_r = \begin{cases} \frac{12.9}{Re_R^{0.5}} + \frac{128.4}{Re_R} & 32 \leq Re_R < 1000 \\ \frac{64\pi}{Re_R} & Re_R < 32, \end{cases} \quad (2.31)$$

Where $Re_R = \frac{\rho D^2 |\Omega_i|}{\mu}$ is the rotational Reynolds number.

2.3.2 Turbulent Dispersion

As the flow is time averaged in the simulations small fluctuations in the velocity field that would have effected particles in the real flow is not present. To account for that a turbulent dispersion force is added to the model. The particles experience not the fluid velocity from the calculated velocity field but [14]

$$u_i = \overline{u_i} + u'_i, \quad (2.32)$$

where the $\overline{u_i}$ is the time averaged velocity and u'_i is an eddy velocity fluctuation, unique for each lagrangian particle. The eddy velocity fluctuation is normally distributed with a zero mean and a standard deviation from the eddy velocity scale, u_e , that is defined as follows for $k - \varepsilon$ turbulence model

$$u_e = \sqrt{\frac{2}{3}k}. \quad (2.33)$$

In the model, u' will then be applied until the eddy interaction time of the fluctuation is over. The eddy interaction time is defined as the minimum of the lifetime of the eddy and the eddy transit time which is the time it takes a particle to flow through it [14].

2.4 Particle-Wall interactions

A particle can interact and collide with walls. In the collision the particle can either stick or rebound from the wall. Interactions of particles with the walls is very complicated as the timescale is very short. There is several different models for modelling the collision, here the Linear Spring model will be briefly explained as an example. The coefficient of restitution determining the amount of lost velocity will also be explained aswell as a model for adhesion.

2.4.1 Linear spring collision model

The Linear spring model consists of a normal and tangential spring-dashpot model with a tangential slider. The normal and tangential forces are defined as [14]:

$$f_n = -K n_n \cdot \delta_n - N_n u_n, \quad (2.34)$$

$$f_t = \begin{cases} -K_t \cdot \delta_t - N_t u_t & \text{if } (|K_t \cdot \delta_t| < |K_n \cdot \delta_n| C_{fs}), \\ \frac{|K_n \cdot \delta_n| C_{fs} \delta_t}{|\delta_t|} & \text{otherwise,} \end{cases} \quad (2.35)$$

where

- K_n and K_t is the normal and tangential spring constant respectively.
- δ_n and δ_t is the normal and tangential deformation distance respectively.
- C_{fs} is the coefficient of static friction.

- $N_n = 2N_{n,damp}\sqrt{K_n M_{eq}}$ where $N_{n,damp}$ is the normal damping coefficient and M_{eq} is the equivalent particle mass.
- $N_t = 2N_{t,damp}\sqrt{K_t M_{eq}}$ where $N_{t,damp}$ is the tangential damping coefficient.

It can be seen in Eq. 2.35 that the tangential force can be calculated in different ways regarding if the particle slides on the wall or if the friction is too high for sliding. The model will induce rotation to the particle but if the friction force is low the particle can slide against the wall making the model physically realistic.

2.4.2 Coefficient of restitution

As particles inelastically collide with the wall some of the kinetic energy of the particle is lost. A common way of describing the inelastic ability of a collision is using the coefficient of restitution. The coefficient of restitution consists of a normal and tangential part and is defined as [17]

$$v_{2,n} = -e_n v_{1,n}, \quad (2.36)$$

$$v_{2,t} = -e_t v_{1,t}, \quad (2.37)$$

where e_i is the coefficient of restitution and the indices $_{n,t}$ denotes the normal and tangential direction and the indices $_{1,2}$ denotes before and after collision respectively.

The coefficient of restitution is measured for different material and impact angles. A study by Reagle et. al. [18] measured the coefficient of restitution for a standard particle, Arizona road dust, of two different sizes and an impact angle between 25° and 85° . A polynomial equation was determined for the larger particles, $20 - 40\mu\text{m}$, of the Arizona road dust on 304 stainless steel depending on the angle of impact:

$$e_t = 1.91 - 0.115\beta + 4.20 \times 10^{-3}\beta^2 - 6.46 \times 10^{-5}\beta^3 + 3.55 \times 10^{-7}\beta^4, \quad (2.38)$$

$$e_n = 1.95 - 0.103\beta + 2.67 \times 10^{-3}\beta^2 - 3.11 \times 10^{-5}\beta^3 + 1.35 \times 10^{-7}\beta^4. \quad (2.39)$$

Where β is the angle of impact. A constant value based on Eqs. (2.38) and (2.39) will be used in the simulations.

2.4.3 Adhesion

When particles approach a wall, different phenomena such as adhesion creates an attraction between the wall and the particle. The physics between this attraction is very complex and research is conducted to find models to accurately model the phenomena [1, 19, 20]. The description of the adhesion process is often done using the DLVO theory, named after Derjaguin-Landau and Verwey-Overbeek. This theory consists of both the van der Waals forces and the forces from the Electrostatic Double-Layer.

The van der Waals forces act on a molecular scale and come from instantaneous fluctuation polarisation of nearby dipoles. The induced dipoles create a covalent attraction between the surface and the particle over small distances. The force is almost always an attractive force, though some examples can be shown where the forces are repelling [1]. The Lifshitz approach to calculating the force treats both bodies as a continuous media instead of treating it on a molecular level as some other methods use.

The Electrostatic Double-Layer force is induced when a charged surface is immersed in a liquid. The force is both attractive and repelling as the distance varies [1]. As the fluid is air in this project the electrostatic double layer will not be present.

Though this model describes the desired physical phenomena well, the computational need is too great for the work in this thesis.

2.5 Cooling package

The cooling package in this study consists of three heat exchangers and a fan. The cooling pack is shown in Figure 2.1 where the grille has been opened. The heat exchangers consist of a radiator, a charge air cooler (CAC) and an oil cooler for the hydraulic fan. As the engine is driving the vehicle forward a lot of heat is produced. The radiator is an air-liquid heat exchanger where the liquid carries the heat from the engine. The

charge air cooler is an air-air heat exchanger. As the turbo is compressing the air, it also gets warmer due to the laws of thermodynamic. A warm air is taking up more space, according to the ideal gas law, see section 2.1.1. As the density is inverse proportional to the temperature a higher temperature leads to a lower density. As the turbos function is to increase the amount of air per space into the engine this is not favorable and the air is therefore cooled in the charge air cooler. The fan is a hydraulic fan that has the function of pulling air through the heat exchangers. As the fan is hydraulic the oil needs to be cooled and therefore there is a third heat exchanger, the oil cooler, which is the smallest of the three. The oil cooler is an air-liquid heat exchanger.



Figure 2.1: *The cooling package, the oilcooler and CAC are visible in the bus and the radiator is behind the CAC. Image courtesy by Volvo Bus.*

The heat exchanger consists of small and thin channels, see the a small part of the radiator in Figure 2.2. The height between the horizontal tubes is about 7.7mm and the width vary from 1 – 2.2mm. The liquid in the radiator is going in the horizontal tubes and the air is flowing through the openings. The reason for the plates between the tubes is to increase the contact area and increase the heat transfer. The CAC and oil cooler looks similar but has a bit larger scales on the slits.

2.5.1 Heat exchanger modelling

As the details of the flow inside the heat exchanger is not of interest, a common way of solving this is to replace the heat exchanger with a porous media in the simulation. The reason for the porous media is to simulate the pressure drop from a heat exchanger while not resolving the details of the flow. The porous media has a resistance which add a term in the fluid momentum equation as [14]

$$s_{p,i} = -P_{ij}^V u_j - P_{ij}^I |u| u_j, \quad (2.40)$$

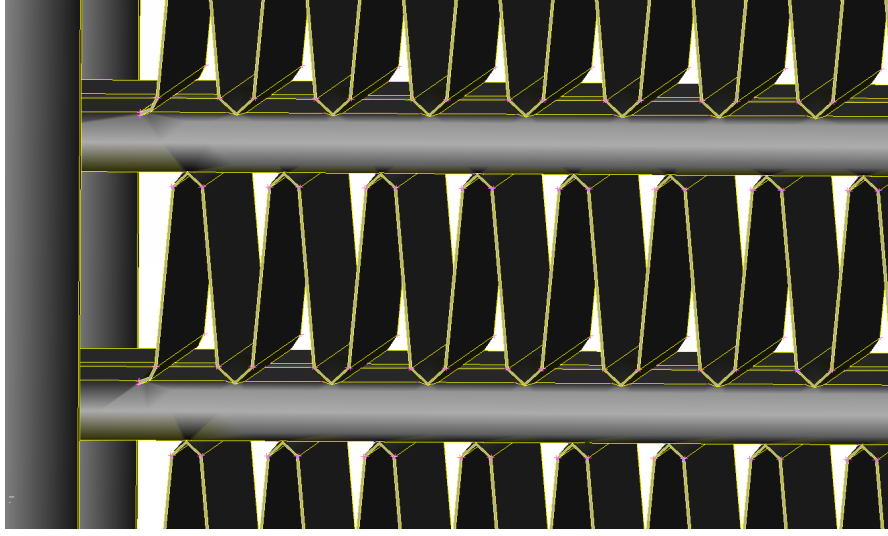


Figure 2.2: A close up on the radiator.

where the P_{ij}^V is the viscous resistance and P_{ij}^I is the inertial resistance. These tensors have to be calculated using data on the performance of the heat exchangers.

2.5.2 Modelling particles in the heat exchangers

The particles are not affected by the same porous resistance as the fluid. A force is applied on the particles in the heat exchanger as

$$F_{resistance} = -a_{ij}u_j - b_{ij}|u|u_j, \quad (2.41)$$

where a_{ij} and b_{ij} are constants chosen to prevent cross directional flow and have been kept zero in the axial direction.

2.6 Modelling rotating objects

In a moving bus parts are moving, such as the fan blades and the wheels. To accurately model the flow around the bus, the movement of these parts need to be addressed. There are different methods of modelling moving objects and the most easily understood method is probably the sliding mesh method where the mesh with the fan blades are rotating. This is a transient method which demands large computational resources. Another way of doing this in a steady framework is the Multiple Reference Frame (MRF) method where the mesh is frozen and the fluid is rotating inside the region. This is obviously a large approximation, but for a steady simulation this method has been shown to be accurate enough for axial fans but with limitations [21].

2.6.1 Modelling Multiple Reference Frame

Multiple Reference Frames or Moving Reference Frame as it sometimes is called is a way of handling moving objects as fans and wheels without moving the mesh, reducing the computational time significantly. The method introduces a rotation in the Navier-Stokes equations as [21, 22, 14].

$$u_{I,k} = u_{R,k} + \varepsilon_{ijk}\Omega_j r_k \quad (2.42)$$

Where the indices I and R is the inertial and rotating frame and the Ω_j is the rotational vector and r_k is the relative position vector from the rotational axis. Starting in the incompressible Navier Stokes equation

$$\frac{du_j}{dt} = -\frac{\partial}{\partial x_j} \left(\frac{p}{\rho} \right) + \nu \frac{\partial^2 u_j}{\partial u_j \partial u_i}, \quad (2.43)$$

and substituting the velocity in Eq. (2.42) into the left hand side of the Eq. (2.43) leads to

$$\left(\frac{du_{I,i}}{dt}\right)_I = \left(\frac{du_{R,i}}{dt}\right)_R + \varepsilon_{ijk} \frac{d\Omega_k}{dt} r_k + 2\varepsilon_{ijk} \Omega_j u_{R,k} + \varepsilon_{ijk} \Omega_j \varepsilon_{klm} \Omega_l r_m \quad (2.44)$$

Where the two last terms represents the Coriolis and centripetal acceleration respectively. When expanding the material derivative for the relative velocity and using that $\frac{\partial}{\partial x_j}(u_{R,i}u_{R,j}) = u_{R,i} \frac{\partial u_{R,j}}{\partial x_j} + u_{R,j} \frac{\partial u_{R,i}}{\partial x_j}$ and that $\nu \frac{\partial^2 u_{I,j}}{\partial u_j \partial u_i} = \nu \frac{\partial^2 u_{R,j}}{\partial u_j \partial u_i}$ the momentum equation for the moving reference frame yields

$$\frac{\partial u_{R,j}}{\partial t} + \frac{\partial}{\partial x_j}(u_{R,i}u_{R,j}) + \varepsilon_{ijk} \frac{d\Omega_k}{dt} r_k + 2\varepsilon_{ijk} \Omega_j u_{R,k} + \varepsilon_{ijk} \Omega_j \varepsilon_{klm} \Omega_l r_m = -\frac{\partial}{\partial x_j} \left(\frac{p}{\rho}\right) + \nu \frac{\partial^2 u_{R,j}}{\partial x_j \partial x_i}. \quad (2.45)$$

But as the interesting velocity will be the absolute velocity and not the relative a change of one of the relative velocities must be preformed in the $\frac{\partial}{\partial x_j}(u_{R,i}u_{R,j})$ term with Eq. (2.42). The final equation that is the one being solved in the simulations follows

$$\frac{\partial u_{I,j}}{\partial t} + \frac{\partial}{\partial x_j}(u_{I,i}u_{R,j}) + \varepsilon_{ijk} \frac{d\Omega_k}{dt} r_k + \varepsilon_{ijk} \Omega_j u_{I,k} = -\frac{\partial}{\partial x_j} \left(\frac{p}{\rho}\right) + \nu \frac{\partial^2 u_{I,j}}{\partial x_j \partial x_i}. \quad (2.46)$$

Limitations of the MRF

One concern with the method regarding this project is that the MRF zone does not affect the particles. The particles will be affected by the drag force from the rotating fluid but no specific contribution from the zone itself exists [14], such as centripetal and Coriolis effects directly. The accuracy of the method can also be a problem and it has been shown that a different defined MRF region can improve the accuracy [21], [23]. It has been shown that a bigger region can produce a more accurate result and that the domain can influence the results. It is necessary for the CFD engineers to be careful to chose an as large domain as possible but always making the same size of the domain [24].

2.7 Volume meshing

A volume mesh is the spatial discretization of the fluid domain and consists of vertices, faces and cells. All CFD simulations are based on a mesh and the mesh has a great influence on the CFD results [25].

2.7.1 Surface wrapping

When the geometry is imported to the CFD software it is usually "dirty" and contains holes, free edges, intersecting and non-manifold surfaces and some unnecessary high level of details. These errors can create errors in the meshing process and need to be taken care of in advance. It is possible to do it manually and go through all the bad section in a pre-processor software but that can be time consuming. Instead a method called surface wrapping is used where a surface is put over the geometry and shrunk to fit the surface with a level of detail that is defined in the settings.

2.7.2 The mesh

Different kind of meshes can be created in most softwares. The most common types of meshes are unstructured meshes that consist of purely tetrahedral cells, mostly hexahedral cells with some tetrahedral or with purely polyhedral cells that is shown in Figure 2.3. Polyhedral meshes are created from tetrahedral meshes which reduces cell count significantly. A polyhedral cell has many faces and a polyhedral mesh provides more accurate results then a mesh with hexahedral cells for the same cell count, though due to its many faces the computational time and memory consumption is higher per cell [25]. Prism cells are often used to better resolve the boundary layer [26]. The prism cells have the same shape as the surface cell but with a height, see Figure 2.4 for examples.

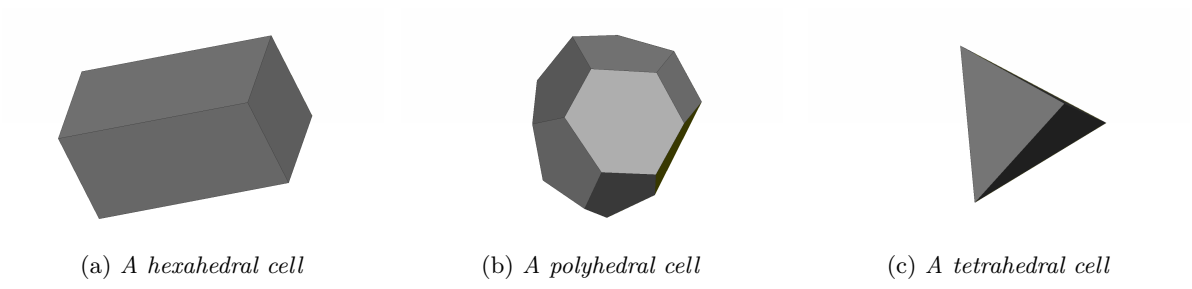


Figure 2.3: *Different kinds of cells*

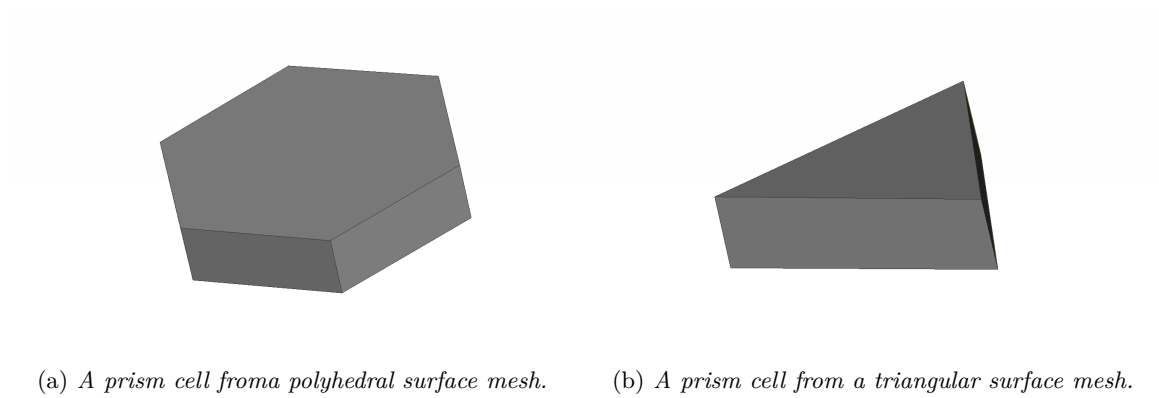


Figure 2.4: *Two different kinds of prism cells.*

3 Method

In this section the software, the process and Case A and Case B will be presented. A case where the effect of rotating particles are evaluated is discribed in the Appendix.

3.1 Softwares

Two main softwares were used in this thesis and will be presented in this section; ANSA for pre-processing and CAD-cleaning and STAR-CCM+ for meshing and simulations.

3.1.1 ANSA

The pre-processor software ANSA by BETA CAE Systems S.A. is a CAE pre-processing tool for CAD-building, CAD-cleaning and meshing. In this thesis ANSA was used to create interfaces for the MRF regions and processing the geometries before meshing.

3.1.2 STAR-CCM+

STAR-CCM+ by CD-Adapco is the CFD-solver used for the thesis. The software is a commercial comprehensive simulation software capable of handling many different physical properties of flow and has an integrated mesher. The software was used from the point the geometry was imported from ANSA and was used to surface wrap, mesh and to calculate the solution to the case. STAR-CCM+ is capable of handling many different physics settings including regions with multiple reference frames, particles and heat exchangers.

3.2 Mesh Generation

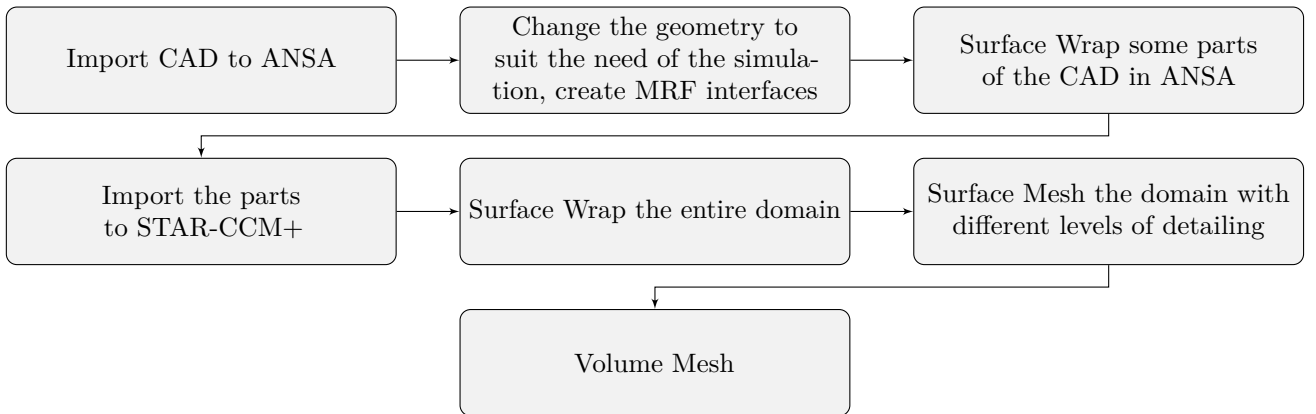


Figure 3.1: *Flowchart of the process of meshing from CAD to volume mesh*

3.2.1 Geometry Preparation

ANSA was used to split up the buses in different part. Some details of the bus is sometimes removed if the details are unnecessary for the specific simulation. For example a towing hitch is unnecessary when analysing the front rounding of a bus. The parts are split into PIDs, as it is called in ANSA to ease the process of creating a good quality mesh and to be able to set appropriate boundary conditions on all surfaces in STAR-CCM+.

3.2.2 Surface Wrapping

Some of the surface wrapping is conducted in ANSA. Some parts, as the engine and the bus cabin are wrapped separately to ensure a good surface quality and that ensure that no hole exists in the parts that would lead to cells occupying empty space. In best case cells occupying empty space slow down the simulations and in worst case it crashes the simulation. The wrapped parts are then imported to STAR-CCM+.

After importing to STAR-CCM+ the parts assigned different regions depending on the physical properties. A porous media has a separate region and the different MRF zones are assigned to different regions. Before the meshing is conducted surface wrapping was applied to improve the quality of the overall surface. The surface wrapping was performed per region. The surface wrapping creates a surface mesh of low quality and the STAR-CCM+'s tool surface remesher is used to improve the quality of the surface mesh.

3.2.3 The Volume mesh

When the surface mesh has a good enough quality the volume mesh is generated. For this kind of geometry and physics properties both STAR-CCM+'s trimmer mesh, which creates a mesh of predominately hexahedral cells with cut cells close to walls, and a polyhedral mesher can create a good quality mesh [14]. More about which mesher that was chosen for each case will be presented in Section 3.6.2 and 3.7.1.

3.3 Setting up multiple reference frames

There are five MRF-zones in this case, four is in the rims of the rear wheels and one is around the fan. Around the zones there are interfaces between the regions. The interface surface has to be copied and put in each of the regions which is then imprinted on each other to create the interface.

3.3.1 Setting up the multiple reference frames at the fan

Around the fan the interface surfaces was set up. The space for the rotating region is limited and the best possible zone is hard to set up. The zone and the fan blades can be seen in Figure 3.2.



Figure 3.2: *The fan blades with the interfaces for the rotating region.*

3.3.2 Turbulence model selection

The selection of turbulence model is a balance on the computational resources available and the need to accurately resolve the flow. The most accurate models are usually time dependent and demands a cell size that is considerably much smaller then the cell size criteria when using a RANS model. For this case the realizable $k - \varepsilon$ model was deemed to resolve the flow sufficiently to be able to accurately understand the particle behavior with a low computational cost. The turbulence model is also the most used model at Volvo Buses and the understanding of the models is high. Close to the wall the STAR-CCM+'s Two-Layer All $y+$ Wall Treatment was used as it is valid for all regions regardless of the cell size in that region. It is a combination of high and low $y+$ value treatment depending on the $y+$ in the specific cell. It is the recommended near wall treatment [14].

3.4 Particle Injectors and Lagrangian solver settings

There are different injectors available in STAR-CCM+, a point injector, a solid cone injector, a hollow cone injector, a part injector and a surface injector. The point is a defined point where a velocity can be applied, the hollow cone has two defined angles for specifying the flow and a diameter. The angles define an inner and an outer limit for the flow and the particles is flown out with a specified velocity randomly from that cone. The solid cone is much the same but without an inner angle, so only a diameter and an outer angle is defined. The part injector and the surface is quite similar, a part is chosen and the parcels can be released from it. A difference between them is that on the part injector a point inclusion probability can be chosen to reduce the number of particles when there is a lot of cells on the surface. On the surface and part injector a specific coordinate system can be chosen as well allowing for parcels to be released tangential from a wheel. The part injector can also be chosen on a constrained plane which is a plane anywhere in the domain.

3.4.1 The dust

In this thesis only dry dust will be studied and the density of the dust has been chosen as 2468kg/m^3 which is the same as silicon dioxide, the largest component of Arizona Road Dust. Arizona Road Dust is a commonly used sand for testing many applications as bouncing and thus have valid data for the substance. It was the substance used for the simulations on coefficient of restitution by Reagle et. al. [18]. The diameter on the particles was a normal distribution with particles from $1 \cdot 10^{-5}$ m to $9.99 \cdot 10^{-3}$ m.

3.4.2 Lagrangian solver settings

The most important settings in the Lagrangian steady solver is the number of substeps, maximum residence time and the Courant numbers. The substeps is the number of iterations (time marching steps) allowed for the particles, maximum residence time is how long the particle is tracked if it is exiting through the outlet and the Courant numbers determines the time steps as shown in Section 2.2.2. The maximum numbers of substeps were chosen to be 25000 though up to 1000000 substeps were tried. The maximum time was set to 50s as it was deemed that if the particle had not reached the outlet after that time it was unlikely that the particle would reach the outlet any time soon after that. The minimum Courant number was set to 0.15 and the maximum 0.45. The Courant number should not be set to high as it can lead to a particle flying through many cells in one step. A particle flying through many cells in one time step can miss certain flow characteristics and can lead to an unphysical solution.

3.5 Solver settings

The solver settings will be presented here. Some of the models are pre chosen by STAR-CCM+ and some are chosen by the user. In Table 3.4 and 3.1 the models for the fluid phase is shown and in Table 3.5 the models for the Lagrangian phase is shown. A steady simulation has been decided to reduce the computational cost and the particle will be simulated with steady Lagrangian without any collisional models. The particles will have a coefficient of restitution applied as $e_n = 0.4$ and $e_t = 0.8$ for the normal and tangential velocities respectively, which corresponds to a wide range of angles from Eqs (2.38) and (2.39) but is not very good for very small or very large angles of attack. The field function restricting the velocities of the particles in the heat exchanger according to Section 2.5.2. On the fan blades, the coefficient of restitution was set to be 1 as a lower value leads to unphysical behavior of the particles.

When running the case the fluid fields were first calculated and the Lagrangian solver was frozen, i.e. no particles are released during the fluid calculations. When the fluid is converged the fluid solver is set to frozen and the Lagrangian solver is run for an iteration. The two-way coupling is turned off so the particles are not effecting the fluid and allowing for this unconnected solution method. The User-Defined Body Force in Table 3.5 is defined as shown in Listing 3.1 based on Eq. (2.41). In the body force 300000 is a large number and has no theoretical base. The question mark in the Listing 3.1 is a ternary operator that makes the user-defined

body force to ask if the particle is in any of the three heat exchanger regions the body force will be active, if not the last line $[0,0,0]$ will be the force on the particles.

```
(({$RegionIndex}==1) ?
[-${ParticleVelocity}[0]*300000 -
mag(${ParticleVelocity})*${ParticleVelocity}[0]*300000 ,
-${ParticleVelocity}[1]*0 -
mag(${ParticleVelocity})*${ParticleVelocity}[1]*0 ,
-${ParticleVelocity}[2]*300000 -
mag(${ParticleVelocity})*${ParticleVelocity}[2]*300000]
: (($RegionIndex==2) ? [-${ParticleVelocity}[0]*300000 -
mag(${ParticleVelocity})*${ParticleVelocity}[0]*300000 ,
-${ParticleVelocity}[1]*0 -
mag(${ParticleVelocity})*${ParticleVelocity}[1]*0 ,
-${ParticleVelocity}[2]*300000 -
mag(${ParticleVelocity})*${ParticleVelocity}[2]*300000]
: (($RegionIndex==3) ? [-${ParticleVelocity}[0]*300000 -
mag(${ParticleVelocity})*${ParticleVelocity}[0]*300000 ,
-${ParticleVelocity}[1]*0 -
mag(${ParticleVelocity})*${ParticleVelocity}[1]*0 ,
-${ParticleVelocity}[2]*300000 -
mag(${ParticleVelocity})*${ParticleVelocity}[2]*300000]
: [0,0,0]))
```

Listing 3.1: Porous Resistance field function

3.6 Case A

While testing how the particles flew in the cooling package, a small geometry setup was used. Using this setup it was possible to test the effect of the different kind of grilles used on Volvo's buses.

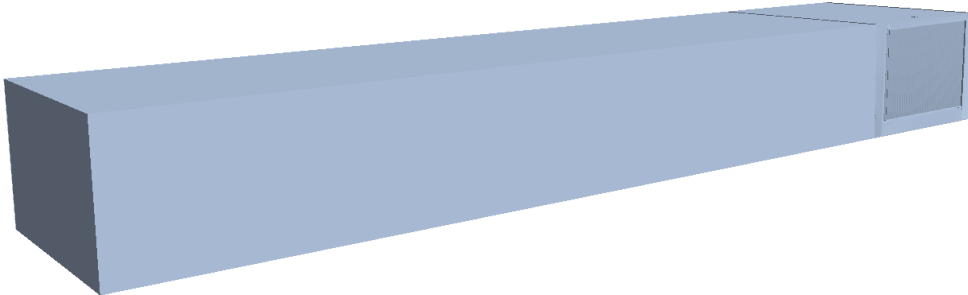
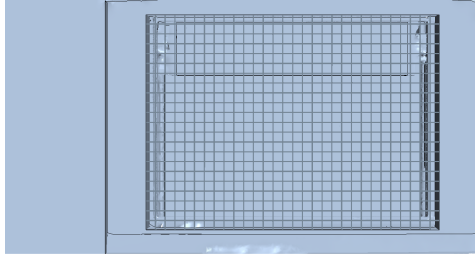


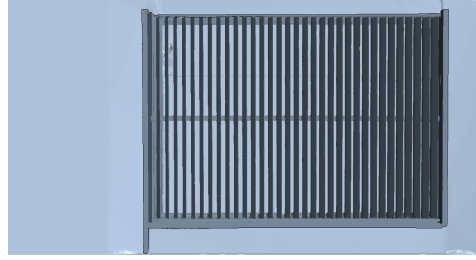
Figure 3.3: *The geometry for for testing smaller cases. Flow from the left.*

3.6.1 Different grilles

Volvo builds their own buses but also lets other companies make their own chassis. A bus body manufacturer have created a different grille that will be tested besides a Volvo grille. While the bus body manufacturer grille seen in Figure 3.4a only is a thin mesh (will be called mesh grille), the original Volvo grill seen in Figure 3.4b has slits that is angled about 45° . The investigation would see if the different grills reduces the amount of particles entering the cooling package. The particles on the original Volvo grill would have to bounce of the grille before getting sucked in, with the coefficient of restitution from Section 2.4.2 applied as $e_n = 0.4$ and $e_t = 0.8$ which is an approximation of the function for angles that are not very small or very large. A case where the Volvo grill was removed was also run.



(a) A grille from a bus body manufacturer, the mesh grille



(b) A grille used by Volvo

Figure 3.4: The tested grills

3.6.2 The mesh and settings for Case A

The mesh for Case A was a polyhedral mesh with hexahedral cells in the heat exchangers. The mesh consisted of 4.4 to 4.7 million cells. Three prism layers were used to resolve the boundary layer. The models in the case is shown in Tables 3.1.

Table 3.1: Models for the air in STAR-CCM+.

| Models selected for the case |
|---------------------------------|
| Cell Quality Remediation |
| Coupled Energy |
| Coupled Flow |
| Gas |
| Gradients |
| Gravity |
| Ideal Gas |
| K-Epsilon Turbulence |
| Lagrangian Multiphase |
| Realizable K-Epsilon Two-Layer |
| Reynolds-Averaged Navier-Stokes |
| Segregated Flow |
| Steady |
| Three Dimensional |
| Turbulent |
| Two-Layer All y+ Wall Treatment |

3.6.3 Initial and boundary conditions

The boundary conditions for the case are listed below in Table 3.2 and the initial conditions will be in Table 3.3.

Table 3.2: The boundary conditions for the case

| Boundary | Boundary condition |
|------------------|--|
| Inlet | Velocity inlet at bus velocity |
| Outlet | Pressure outlet |
| Sides and top | Symmetry plane |
| Ground | No-slip wall with bus velocity prescribed velocity |
| All of the boxes | No-slip wall |

Table 3.3: The boundary conditions for the case

| | Initial value |
|---------------------------|-----------------------------|
| Pressure | 0Pa |
| Turbulence Intensity | 0.002 |
| Turbulence Specification | Intensity + Viscosity Ratio |
| Turbulent Velocity Scale | 10m/s |
| Turbulent Viscosity Ratio | 200 |
| Velocity | [1.0, 0, 0]m/s |

In the heat exchanger regions, a porous media resistance is added, where the values is been calculated using data of the heat exchanger. A very high value is set in the cross-stream direction is to make sure the flow is in purely in the axial direction axial direction, i.e. straight though the heat exchangers seen in Figure 2.2. The pressure defined as 0Pa in Table 3.3 is pressure above the atmospheric pressure.

3.6.4 Particle injector

The particle injector for Case A was chosen to be a hollowed cone with inner and outer angle of 30° and 35° respectively. The number of particles released was 500 which gave a wide variation of the diameter in the normal distribution mentioned in Section 3.4.1.

3.7 Case B

The geometry for this case is a full detailed Volvo 9700 bus with eight wheels, the first of the rear wheels have two wheels on each side. The surface wrapper removes some of the smallest detail for an easier volume mesh but no part of the bus is removed beforehand.

3.7.1 Mesh for Case B

For this case the trimmer mesh was used for the largest airstream domain due to the complexity and the high levels of geometrical details, and a polyhedral mesher inside the MRF-zones where the fluid is rotating. The mesh consisted of a total of 36.7 million cells and Figure 3.5 shows a close up of the mesh around the bus. Before, under and behind the bus as well as around the grille and in the engine compartment there is refinement boxes where most of the 36.7 million cells are located. The growth rate is set to 1.8 which is quite fast but works well for this case when the interesting region has refinement boxes with isotropic cells. On most surfaces 5 prism layers were used. In the engine compartment only one layer was used to reduce the cell count.

3.7.2 Setting up the multiple reference frames at the wheels

The multiple reference frames around the wheel is only inside the wheel, where the rim is. The interfaces was created to include as much as the rotating part as possible, without adding stationary parts, as the brakes. As any part put in the MRF zone would be modelled as rotating the brakes was put outside the interface even though some of the rim was left outside the zone. As can be seen in the Figure 3.6 some of the wheels are double. Between these double wheel a MRF interface was created to allow for the fluid between the wheel to be rotating. The rotating speed of the wheels was calculated based on their diameter and the speed of the bus and with a speed of 90kph the rotating speed was set to 420rpm.

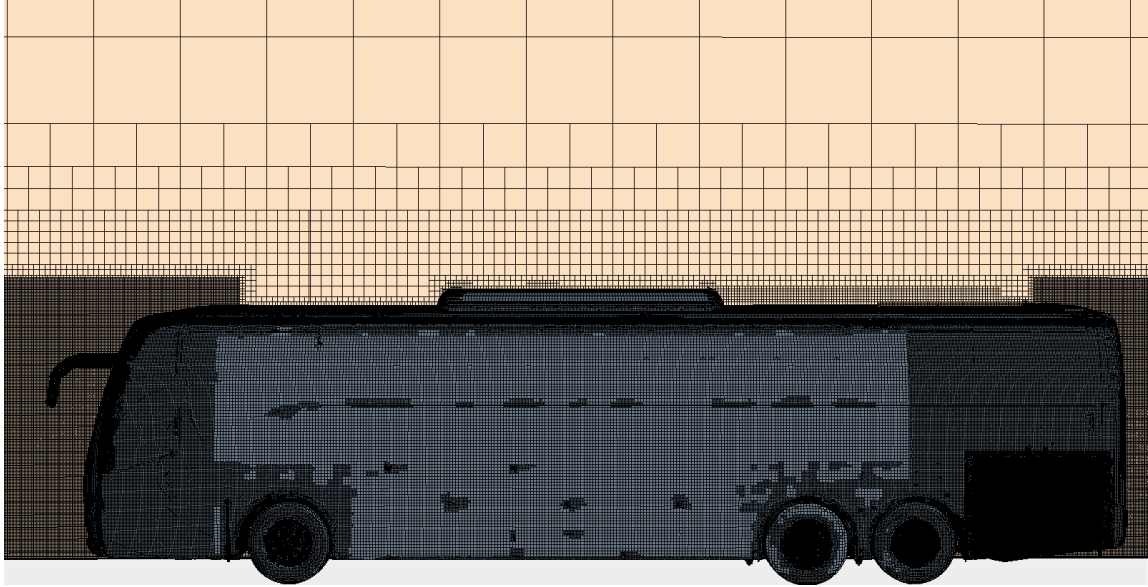
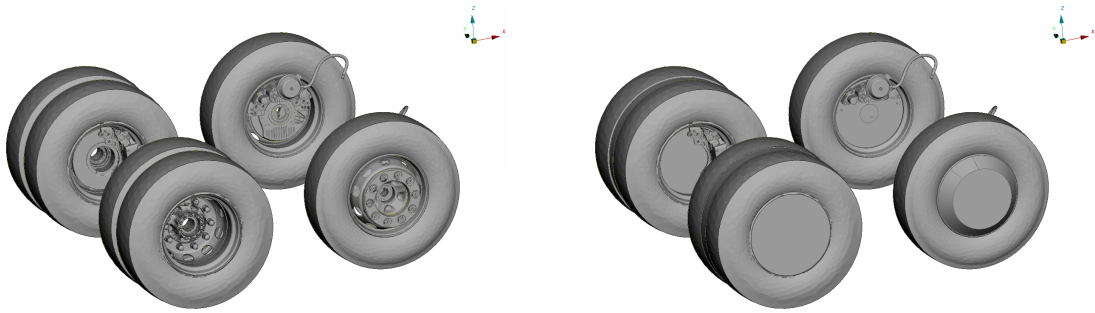


Figure 3.5: *The mesh on and around the bus.*



(a) *The wheels without the MRF zones.*

(b) *The wheels with the MRF interfaces.*

Figure 3.6: *The wheels with and with out the MRF interfaces*

Table 3.4: Models for the air in STAR-CCM+.

| Models selected for the case |
|------------------------------------|
| Cell Quality Remediation |
| Constant Density |
| Gas |
| Gradients |
| K-Epsilon Turbulence |
| Lagrangian Multiphase |
| Realizable K-Epsilon Two-Layer |
| Reynolds-Averaged Navier-Stokes |
| Segregated Flow |
| Steady |
| Three Dimensional |
| Turbulent |
| Two-Layer All y^+ Wall Treatment |

Table 3.5: Models for the Lagrangian phase in STAR-CCM+

| Lagrangian models selected for the case |
|---|
| Constant Density |
| Drag Force |
| Material Particles |
| Pressure Gradient Force |
| Residence Time |
| Solid |
| Spherical Particles |
| Track File |
| User-Defined Body Force |

Table 3.6: The different injectors and their settings.

| Injectors | Type | Velocity | Number of parcels |
|----------------------|----------------------------------|-------------------|-------------------|
| In front of bus | Part inj. on a surface | [90, 0, 0] kph | 490 |
| Under bus | Part inj. on a surface | [90, 0, 4] kph | 430 |
| The front rear wheel | Part inj. on a constrained plane | 90 kph tangential | 375 |
| The rear rear wheel | Part inj. on a constrained plane | 90 kph tangential | 300 |

3.7.3 Particle Injectors and settings

In Table 3.6 the injector under the bus has a velocity component in the z-direction as well as the x-direction. This to assure that the particles moves upwards and interact with the bus and the flow under the bus. The point inclusion probability was used on all injectors was as low as 1% and 2% on the first and second rear wheel respectively. 5 parcels was released from each point to get a dispersion of the particle diameters. A case will also be run where the coefficient of restitution are changed to $e_n = e_t = 0$ so the particles will get stuck if they hit the engine to see if it is possible to analyze accumulation of dirt in the engine compartment.

3.7.4 Initial and boundary conditions

The boundary conditions for the case is listed below in Table 3.7 and the initial conditions will be in Table 3.8.

Table 3.7: The boundary conditions for the case

| Boundary | Boundary condition |
|----------------------------------|---|
| Inlet | Velocity inlet at 90kph |
| Outlet | Pressure outlet |
| Sides and top | Symmetry plane |
| Ground | No-slip wall with 90kph prescribed velocity |
| All of the bus except the wheels | No-slip wall |
| The wheels | Rotating boundary condition at 420 rpm |

Table 3.8: The boundary conditions for the case

| | Initial value |
|---------------------------|-----------------------------|
| Pressure | 0Pa |
| Turbulence Intensity | 0.002 |
| Turbulence Specification | Intensity + Viscosity Ratio |
| Turbulent Velocity Scale | 10m/s |
| Turbulent Viscosity Ratio | 200 |
| Velocity | [1.0, 0, 0]m/s |

In the heat exchanger regions, a porous media resistance is added, where the values is been calculated using data of the heat exchanger. A very high value is set in the cross-stream direction is to make sure the flow is in axial direction. The pressure defined as 0Pa is pressure above the atmospheric pressure.

3.7.5 Calculating the path of the particles

For calculating how many particles that fly through the engine compartment some constrained planes are set up. The planes covers the major known in and outlets of the engine compartment to calculate the flow of particles. Caution has to be taken to ensure that the constrained plane is the correct one, the plane will consists of all cells inside the border so even if just a corner of a cell is in the border it will be a part of the constrained plane.

4 Results

In this section the results will be presented. The result from the Case A that was described in Section 3.6 is presented first. Case B with the whole bus described in Section 3.7 will be presented after that. The result from the rotating test is located in the Appendix A.

4.1 Case A

The smaller case was run to test different models of grilles and to test the behaviour of the particles through the cooling package and some interesting results can be seen from this case.

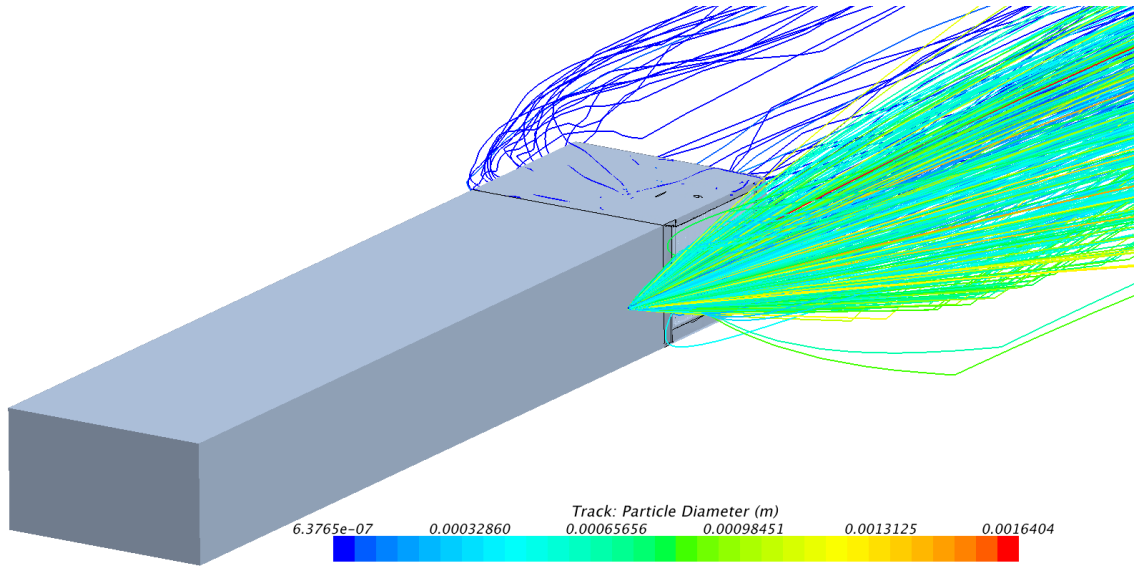


Figure 4.1: *Particles getting sucked into the cooling pack colored by their diameter.*

In Figure 4.1 the particles are released in front of the air intake and it can be seen that mostly the smaller particles are sucked into the cooling package. The blue lines on the roof of the box is a visualisation bug, they only hit the wall on the inside. In Figure 4.2 it can be seen that the larger particles hit the grille and bounce away from the intake. The small particles bounce as well but with their lesser momentum they still can be sucked into the cooling package.

In the Figure 4.3 the particle behavior inside the heat exchanger is illustrated, the particles go through the heat exchangers in a straight line and not cross-wise due to the user defined function in Listing 3.1. In the Figure 4.4 the particles can be seen after the fan together with streamlines, that are thinner and more transparent than the particle tracks. It can be seen that the velocities are much larger right after the fan but the overall behavior after the fan are similar and the velocities are similar a short distance from the fan.

The Table 4.1 shows the diameter and the ratio of particles released that enters the cooling package. It can be seen that a higher speed leads to less particles and that the mesh grille both gets more particles but also an increase in the mass flow of air. The largest difference is on the size of the particles that goes through. The largest size of the particles is over 5 times as large for the 30kph case and 7 times as large for the 90kph case.

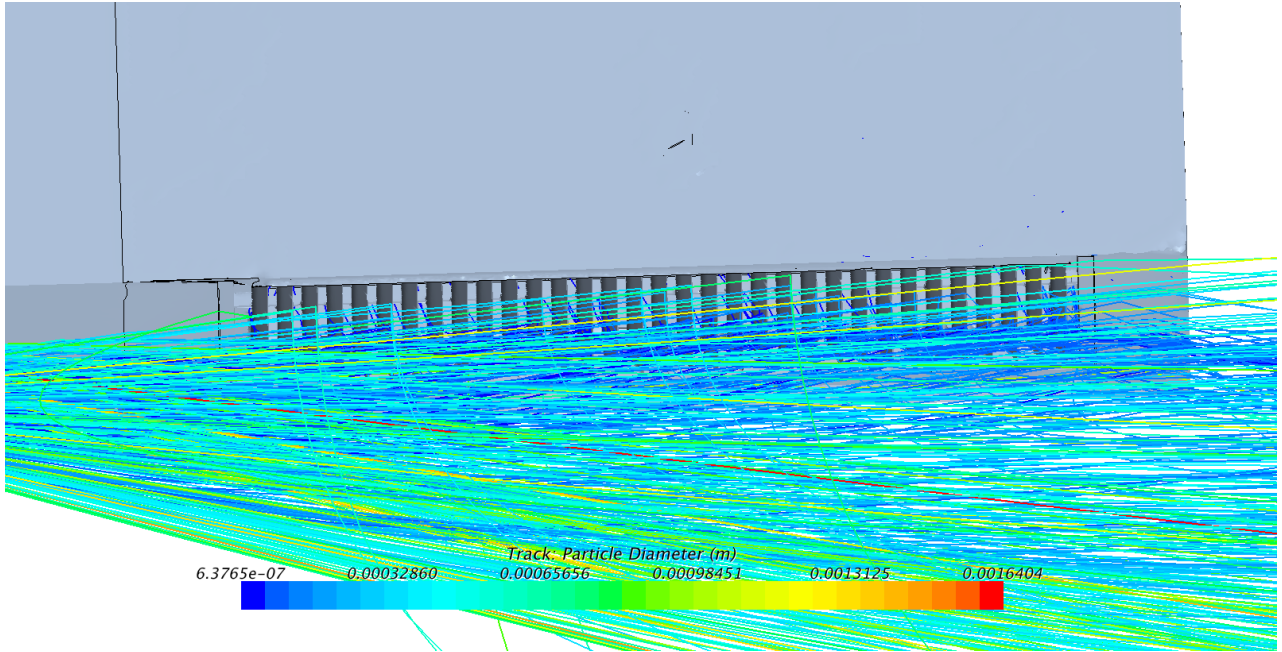


Figure 4.2: *Particles bouncing the grille.*

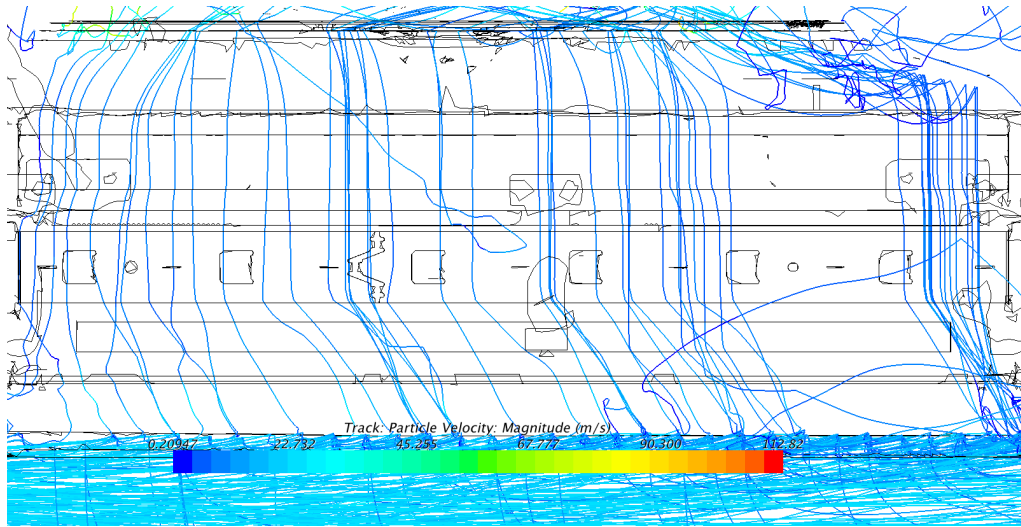


Figure 4.3: *Particles getting through the heat exchangers colored by their velocity.*

Table 4.1: The two different grilles at two speed each, the fans are at the same speed for all cases

| | Volvo grille, 30kph | Volvo grille, 90kph | Mesh grille, 30kph | Mesh grille, 90kph |
|---|---------------------|---------------------|--------------------|--------------------|
| Max diameter | 0.24mm | 0.14mm | 1.04mm | 0.98mm |
| Ratio of particles in fan of released particles | 27.4% | 8.6% | 53% | 45.9% |
| Massflow changes | Reference | -6.4% | +18.1% | +14.8% |

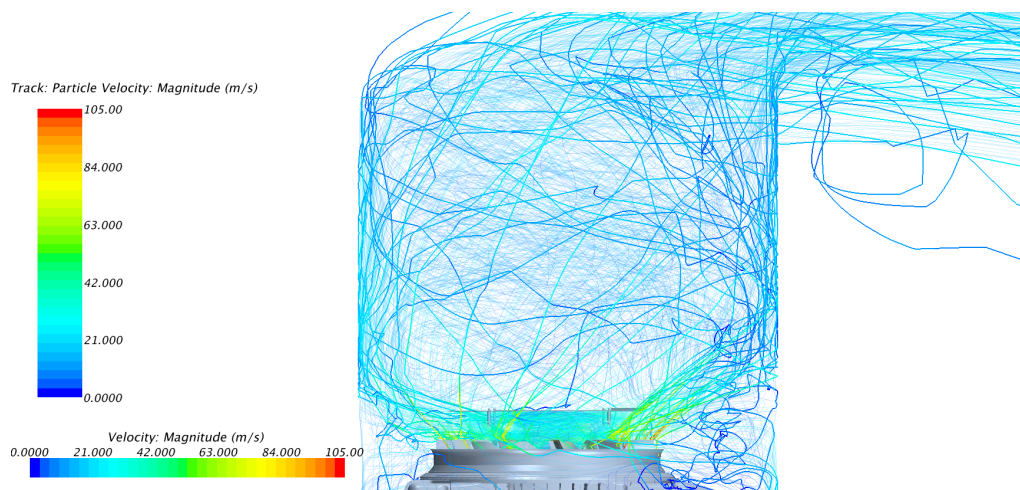


Figure 4.4: *Particles and fluid streamlines coming out of fan.*

4.2 Case B

In the case with the complete bus the fluid flow was run with the Lagrangian particles "frozen", i.e. no particles were released during these iterations. The particles are released as a post-processing step from the injector as described in the Section 3.4. In the Figure 4.5 the particles are released only from the wheels and their path can be seen from the wheels to the outlet. Note that there are particles that goes under the bus to the opposite side from where they are released so not all particles will flow over the air intake. The Tables 4.2 to 4.5 shows the number of particles entering and exiting the engine compartment. A stuck particle is a particle that have not reached the outlet either after the substepping is finished or the maximum residence time have passed.

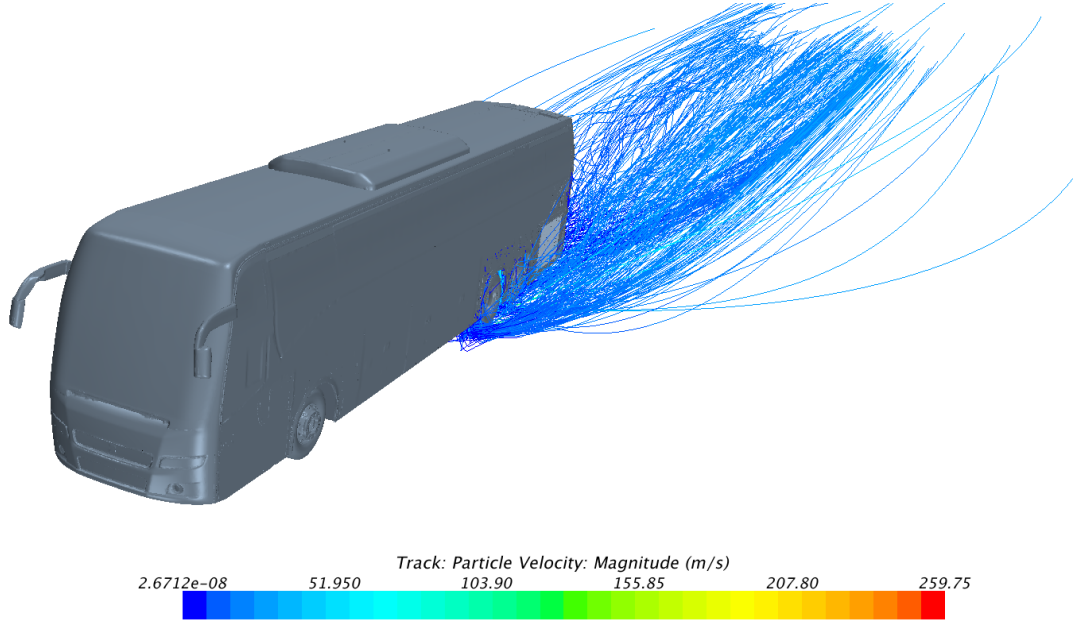


Figure 4.5: *The particles around the bus, only released from wheels on the left side of the bus.*

Table 4.2: The results from the particles released from the constrained planes with bouncing particles in the engine compartment.

| | In front of the bus | Under the bus |
|-----------------------------------|---------------------|---------------|
| Released parcels | 490 | 430 |
| Through the grille | 0 | 0 |
| Through the opposite grille (out) | 0 | 0 |
| Through the back grille (out) | 0 | 1 |
| Stuck Particles | 0 | 123 |

Figure 4.6 shows particles bouncing of the grille and only a few enters, more about this in Section 4.1. The Figure 4.7 shows particles when the coefficient of restitution for the engine part are set to zero, causing particles getting stuck where they hit the part. In Figure 4.8 particles that are caught under the wheels are shown colored by the velocity.

In the Figure 4.9 the particles paths into, in and out of the engine compartment can be seen. It can be seen that most of diameters are represented in the engine compartment. The largest particle in the compartment is 1.13mm in diameter. It can also been seen in Figure 4.9 that some particles enter from the gearbox where a small opening around the box exists.

Table 4.3: The results from the particles released from the wheels with bouncing particles in the engine compartment.

| | The first rear wheel | The second rear wheel |
|---------------------------------|----------------------|-----------------------|
| Released parcels | 375 | 300 |
| In through the grille | 1 | 0 |
| Out through the grille | 2 | 0 |
| In through the opposite grille | 0 | 0 |
| Out through the opposite grille | 1 | 0 |
| In through the back grille | 2 | 1 |
| Out through the back grille | 1 | 1 |
| Stuck Particles | 125 | 77 |

Table 4.4: The results from the particles released from the constrained planes where particles get stuck to the engine when hit.

| | In front of the bus | Under the bus |
|-----------------------------|---------------------|---------------|
| Released parcels | 490 | 430 |
| Through the grille | 0 | 0 |
| Through the opposite grille | 0 | 0 |
| Through the back grille | 0 | 0 |
| Stuck Particles | 0 | 125 |

Table 4.5: The results from the particles released from from the constrained planes where particles get stuck to the engine when hit.

| | The first rear wheel | The second rear wheel |
|---------------------------------|----------------------|-----------------------|
| Released parcels | 375 | 300 |
| In through the grille | 0 | 0 |
| Out through the grille | 0 | 1 |
| Out through the opposite grille | 0 | 0 |
| In through the opposite grille | 0 | 0 |
| Out through the back grille | 0 | 1 |
| In through the back grille | 0 | 1 |
| Stuck Particles | 127 | 95 |

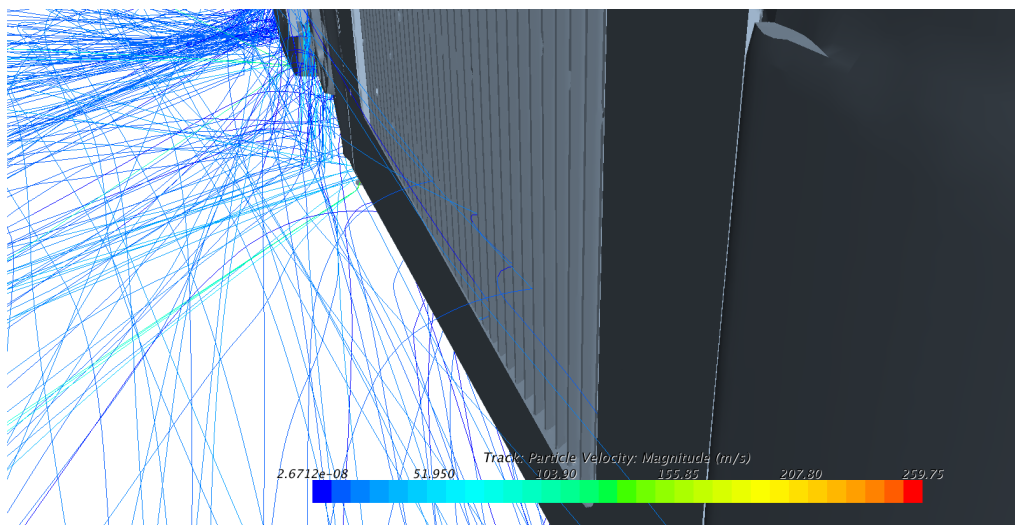


Figure 4.6: *Particles bouncing of the grille.*

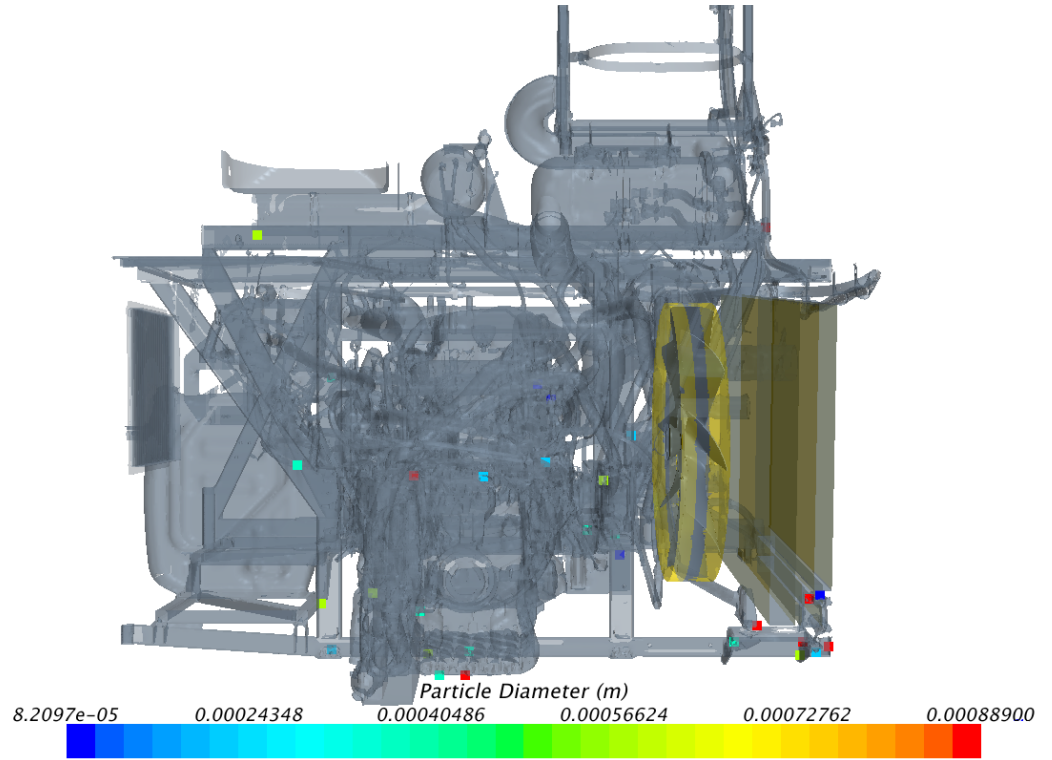


Figure 4.7: *Particles that are stuck in the engine. The opposite grille are shown on the left side of the figure. Colored by their diameter*

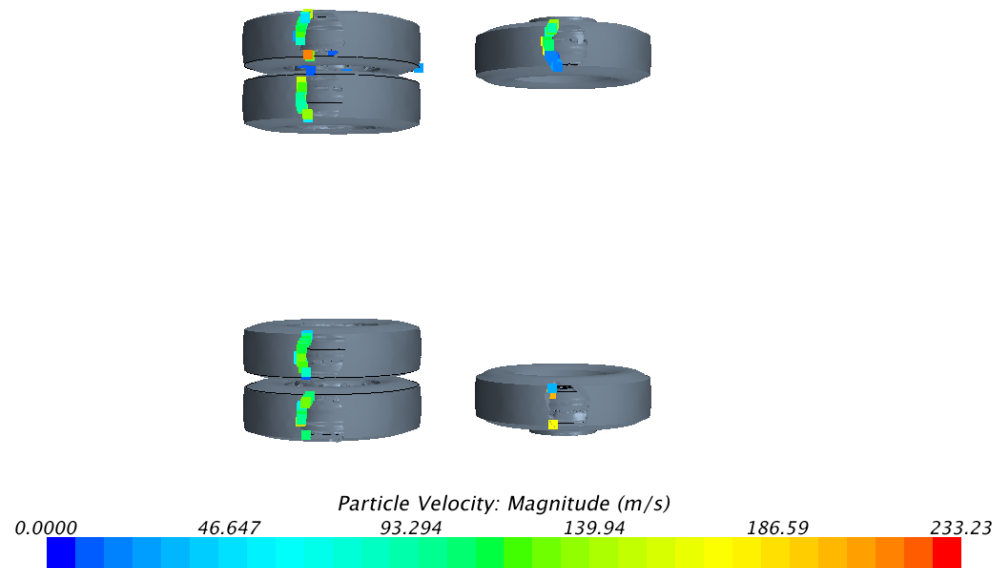


Figure 4.8: *Particles getting stuck under the wheel, view from below. Colored by the velocity.*

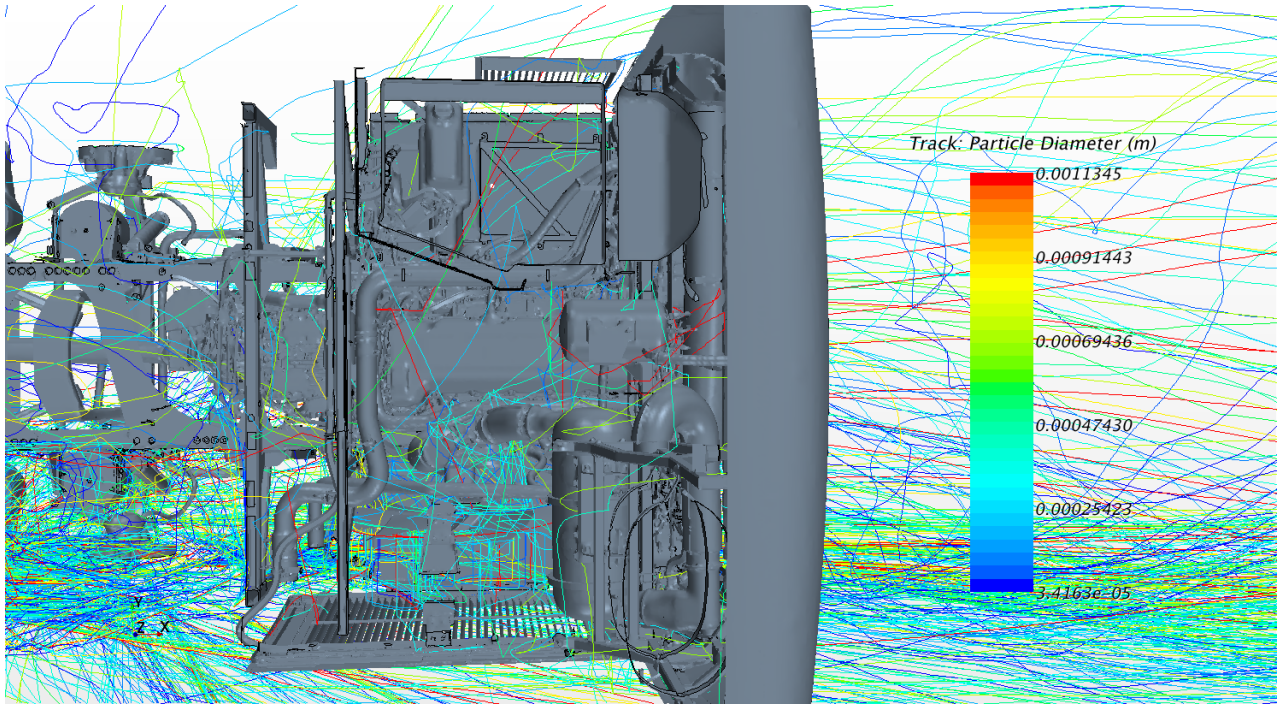


Figure 4.9: *Particles path from the rear wheel into the engine compartment and then out again. Colored by the particle diameter.*

It can be seen in Figure 4.10 that some of the particles hit the constrained plane used to count particles in the wrong direction. In the figure, it is seen how a particle emerges out of the grille from an unknown source, possible the gearbox, and then get sucked back in.

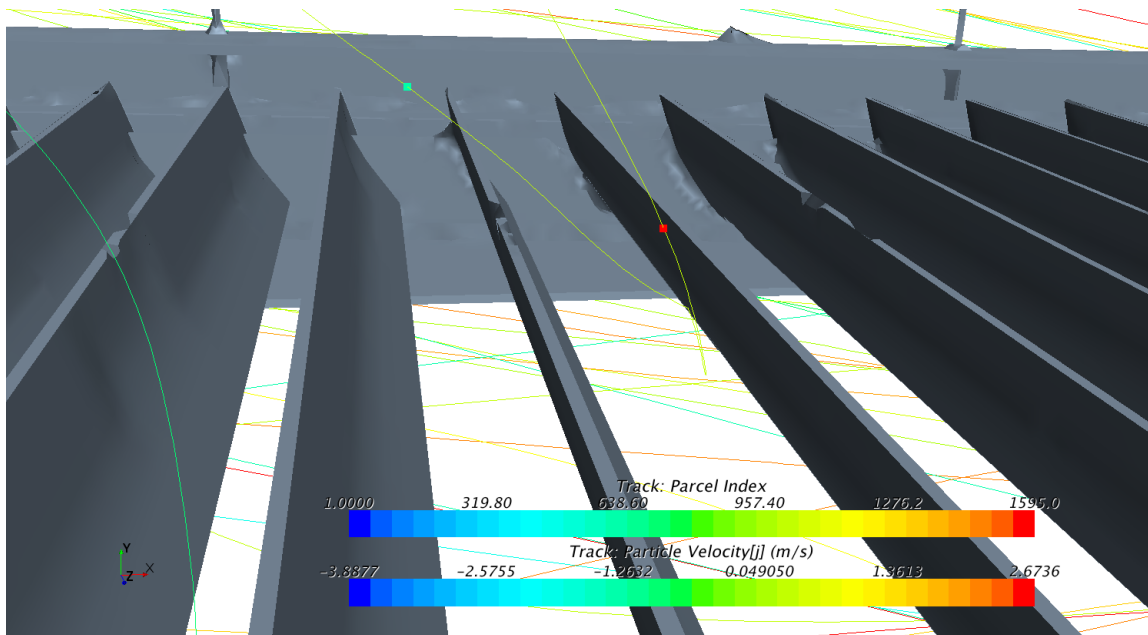


Figure 4.10: *Particles seen exiting and entering the grille in the engine compartment. The track is colored by the Parcel Index and the dot by the velocity in the y-direction. The engine is located above the figure.*

In the Figure 4.11 the residence time of the particles that are stuck in the domain is shown. Some particles have the maximum 50s residence time and have been stuck due to that. But it can be seen that most of the particles have a residence time to the power of -5 indicating that the number substeps was the reason for the particles being stuck in the domain. It was tried to increase the number of substeps to 1000000 to get the particle a chance to exit the domain but most of the particles that was stuck under the wheel remained under the wheel even when increasing the substeps.

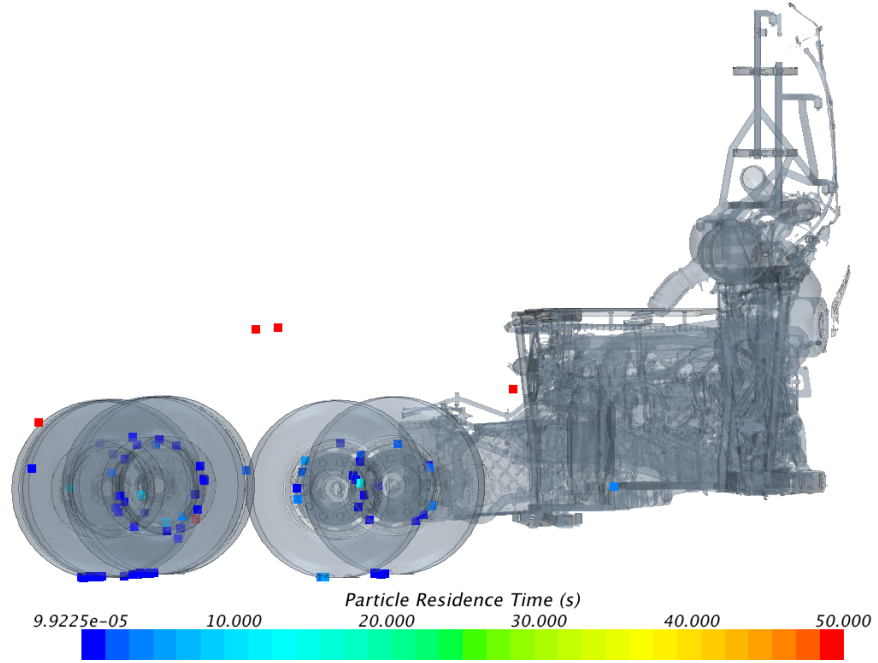


Figure 4.11: *Particles that are still left in the domain after tracking, with bouncing in the engine. Colored by the residence time.*

5 Discussion

In this section the presented results and the method with its limitations will be discussed.

5.1 Case A

It can be noted in Table 4.1 that when using the Volvo grille less particles pass through through the cooling package. One reason for this is of course the lower mass flow of air through the cooling package but a large portion is also, as was noted in the Figure 1.1, that the particles must hit the walls of the grille before entering the cooling package making a large portion of the particles bounce of as shown in Figure 4.2.

5.1.1 Particle diameter through the grille

It can be seen that larger particles get through the grille in the case with the complete bus as compared to having the Volvo grille on the test case. It should be noted that the grilles are not identical, although they are quite similar. A possible reason for this is the complex flow from the wheel house that is a lot more turbulent than the flow over the geometry in the Figure 3.3. An interesting observation is that the largest particles seem to be influenced the most by the bouncing effect and not entering after bouncing of the grille. This makes the Volvo grille much better at preventing large particles entering than the mesh grille. An analysis of the airflow and the effect needed for the fan must also be taken into account as the Volvo grille requires more effect to be able to provide the same mass flow through the cooling package.

5.1.2 The cooling package

The particles are crossing the heat exchangers and the user-defined field function from List 3.1 appears to yield the desired behavior. The cross-stream velocities are terminated and only the velocity component in the axial direction is kept and it is only the flow in the axial direction that affects the particles as shown in Figure 4.3.

On the fan blades the coefficient of restitution was set to be 1 and not the values from Reagle et al. [18]. The reason for this was the unphysical behavior of the particle when loosing momentum in the hit. As the model is not allowing the particle to roll on the blade as it would do otherwise and the fluid in the MRF zone is pushing the particles repeatedly against the blade and momentum is lost every hit. This leads to an unphysical behavior as the particles loose so much momentum the velocity is approaching zero and the particle get stuck there.

5.2 Case B

In Case B it is interesting that hardly any particles get sucked into the engine compartment as can be seen in Table 4.2 and Table 4.3. It can be seen in Tables 4.4 and Table 4.5 that no particles exits through the grille on the opposite side when bouncing is turned off. If the particles not get stuck on the engine they exits the rear grille which have a more straight way without many obstacles. The number of particles entering the engine suggests that more particles are needed for a better representation of the situation.

When looking at Figure 4.7 it is hard to see any evident trends in where the particle sticks. The number of particles entering the engine compartment is to few to accurately analyze this where they will stick. It can be seen that a lot of particles have got stuck at the gear box and due to that less particles seems to enter the engine compartment as many particles enter from the gap there. Some particles got stuck far to the right in the figure as well, in the side of the heat exchangers where the fluid velocity is very low and possible the particles get stuck in that stagnant zone.

5.2.1 Entering and exiting the engine compartment

As seen in Tables 4.2 to 4.5 the number of particles that enter and exits the engine compartment does not add up. Planes for monitoring the particles were set up only at the large grille, the grille at the backside and the grille at the opposite side as the air intake. It can be seen in Figure 4.9 that some particles are entering the engine compartment around the gear box, this might be the largest inlet of particles and it looks as more particles are exiting through the air intake than entering. The counting of the particles are very hard as the particles are bouncing and many particles were counted double or more times as seen in Figure 4.10. This makes it important to view the pictures of the particles as well as counting the numbers of particles entering and exiting the planes at the inlet/outlet of the engine compartment.

5.2.2 Particles under the wheels

In Figure 4.8 some particles that are stuck under the wheels are shown and in the Figure 4.11 the residence time is shown. This is not physically correct and on a real moving bus no particles will be stuck under the wheels. In Eq. (2.26) the equation for the time step is shown and it is proportional to the cell size and inversely proportional to the velocity. These particles that have a very low residence time, have a high velocity and are located in the prism cells between the ground and the wheel. The velocity is very high due to the combined prescribed boundary condition at the ground of 90kph and the wheels rotational boundary condition at 420rpm. The reason that the particles are not seeming to leave the domain is probable due to their high velocity in the small cells. As the results did not change after 1000000 sub steps this indicates that the time steps are so small that the particles are unlikely to leave the domain even after unrealistically high number of sub steps.

5.3 Limitations

It is important to have the limitations of the model in mind while looking at the results. When comparing the Figures A.3 and A.2 it can be seen that the angle after a collision with a wall differs quite a lot which indicates that after the particles have collided with a wall they will not have the correct direction. As the particles often collide with the wheel house wall and the grille before entering the engine compartment where they often collide with an engine part this is probably significant.

In the fan the MRF zone are not directly affecting the particles as discussed in Section 2.6.1. It is possible that the direction and even location of the particles out of the MRF zone is not correct. It is possible that this does not affect the results that much as Figure 4.4 shows that the behavior of the particles appears to be close to the streamline, as expected for small particles.

The number of particles is a great concern. The number must be kept low for computational reasons, but the soiling of an engine compartment is not a fast process. The engine compartment is not dirty after just a couple of hours and the number of particles that do enter the compartment is only a few percent of the released particles as seen in Tables 4.2 and 4.3. To get a statistically correct answer if the particles are likely to accumulate somewhere more particles has to be released which will increase the computational demand greatly.

5.4 Computational demands

There is always a consideration on how much computational resources every project can be assigned. The amount of different models must be taken into account when this consideration is done. It would for example be good to take the rotation and collisions into account, but considering the computational time it is not possible to take those models into account.

5.4.1 Adding extra models

This project was conducted in steady simulations to decrease the computational demands. A case where different models were tested are located in the Appendix. As shown in Figure A.2, only changing to unsteady makes no major effect on the results for the bouncing. Though if unsteady simulations are performed the MRF zone can be switched to a sliding mesh which will affect the particle in a more physical way than the MRF zone. Though a sliding mesh demands more computational time than just adding time dependency. For every time step the interface between the regions have to be updated which makes the model even more computationally heavy then the Figure A.3 would suggest.

The best way of solving this case would be to use the DEM mode and adding correct behavior for collision and rotation as well as a linear cohesion models that take Van der Waals forces into account. As DEM mode without linear cohesion increases the time with 5200 factor as shown in Table A.3 the extra computational time would be extreme.

5.4.2 Particle tracks

Tracking particles creates large track files, the first tries of simulations created files over 30GB. These files can be difficult to load and the softwares have crashed when the files are being loaded. Great care has to be taken to have as few particles and number of substeps possible for the analysis of the simulation which made it hard as a large number of particles released from the entire wheel is essential to analyse the flow though the engine compartment as a visualization of the results often can be important. If a transient method is utilized the track files are not necessary and but it increases for the need of correct and clever calculation method as the particles fly into and out of the engine compartment. This can make a problem as it is seen in Tables 4.2 to 4.5 that few particles entering the engine compartment and more would preferably be released making the post processing hard.

5.5 Use of method

The method can be improved. Especially without physical testing of the process of dirt entering the engine compartment, the method should not be used to analyze the path of the particles in the engine compartment. The method works best to analyze possible means of reducing the inlet to the engine compartment like changing grilles, covering the wheel houses or covering the gaps in the covers around the compartment.

5.6 Proposed future studies

Before utilizing the method some suggestions to validate the method is suggested here:

- Physical test should be performed to validate the results.
- Investigate the results of having wet particles and water entering the cooling package.
- Try using an unsteady simulation with a sliding mesh at the fan to examine the error while using a MRF zone and to see if it can be an alternative to use steady calculations with MRF.

6 Conclusions

A method for investigating particle flows around and entering into the engine compartment has been successfully developed. The method consists of solving a flow field first. The heat exchangers in the cooling package are modelled as porous media, and the rotation of the fans is modelled using the MRF technique. When the simulation of the flow field is converged the fluid solver is frozen and the particles are released and tracked in a post-processing step. The particles are released in a steady state Lagrangian framework. In order to make the behavior of the particles in the porous media correspond to the behavior of particles in real heat exchangers, a novel body force acting on the particles in these regions was proposed and implemented in the present work.

The developed method was demonstrated for two cases. The first case with a simple box in front of the cooling package was conducted with releasing particles in front of the intake to a cooling package of a bus. The behavior of particles was analyzed through the cooling package. Two different grilles were tested in this case; a Volvo grille and another grille from a bus body manufacturer. It was seen that the particle bounced off the Volvo grille before entering and the other grille was tested to analyze the impact of the different grilles. The angled grille from Volvo was seen to reduce the number of particles entering the air intake and the diameter of the particles entered was smaller than with grille from the bus body manufacturer that only was a thin mesh.

The second case that the method was demonstrated on was a fully detailed Volvo 9700 bus. Here particles were released in front, under and from the wheels. It was shown that few particles entered through the grille and more particles entered at the gap by the gearbox.

It was concluded that the method works to determine the relative amount of particles entering the engine compartment depending on the bus speed, geometries around the engine compartment and size distribution of particles but that the levels of uncertainty is still too large to accurately analyze the particle path inside the engine compartment.

References

- [1] C. Henry, J.-P. Minier, and G. Lefèvre. Towards a description of particulate fouling: From single particle deposition to clogging. *Advances in Colloid and Interface Science* **185–186** (2012), 34–76. ISSN: 0001-8686. URL: <http://www.sciencedirect.com/science/article/pii/S0001868612001418>.
- [2] T. Cowell and D. Cross. *Airside Fouling of Internal Combustion Engine Radiators*. Tech. rep. SAE Technical Paper, 1980.
- [3] T. Bott and C. Bemrose. Particulate fouling on the gas-side of finned tube heat exchangers. *Journal of Heat Transfer* **105.1** (1983), 178–183.
- [4] Z. Pusheng et al. *Characterization of paved road dust in urban area*. Tech. rep. Institute of Urban Meteorology, China Meteorological Administration, 2006.
- [5] A. P. Gaylard and B. Duncan. *Simulation of Rear Glass and Body Side Vehicle Soiling by Road Sprays*. Tech. rep. SAE Technical Paper, 2011.
- [6] K. R. Cooper. *The effect of front-edge rounding and rear-edge shaping on the aerodynamic drag of bluff vehicles in ground proximity*. Tech. rep. SAE Technical Paper, 1985.
- [7] H. Götz. “Chapter 9 - Commercial vehicles”. *Aerodynamics of Road Vehicles*. Ed. by W.-H. Hucho. SAE International, 1998. ISBN: 978-0-7680-0029-0.
- [8] A. Vdovin. “Investigation of Aerodynamic Resistance of Rotating Wheels on Passenger Cars”. Licentiate Thesis. Chalmers University of Technology, 2013.
- [9] S. Krajnovic, S. Sarmast, and B. Basara. Numerical Investigation of the Flow Around a Simplified Wheel in a Wheelhouse. *Journal of Fluids Engineering* **133** (11 2011), 111001. ISSN: 0098-2202.
- [10] L. Larsson, T. Wiklund, and L. Löfdahl. “Cooling Performance Investigation of a Rear Mounted Cooling Package for Heavy Vehicles”. *SAE World Congress 2011, 12-14 April, Detroit, USA*. 2011.
- [11] W. K. George. *Lectures in Turbulence for the 21st Century*. 2013. URL: http://www.turbulence-online.com/Publications/Lecture_Notes/Turbulence_Lille/TB_16January2013.pdf.
- [12] L. Davidson. “Fluid mechanics, turbulent flow and turbulence modeling”. 2014. URL: http://www.tfd.chalmers.se/~lada/postscript_files/solids-and-fluids_turbulent-flow_turbulence-modelling.pdf.
- [13] H. Versteeg and W. Malalasekera. *An introduction to computational fluid dynamics, the Finite Volume Method*, Pearson Education Limited, 2007.
- [14] *Star-CCM+ User Guide*. v9.06. CD-Adapco. 2015.
- [15] T.-H. Shih et al. A new k- eddy viscosity model for high reynolds number turbulent flows. *Computers & Fluids* **24.3** (1995), 227–238. ISSN: 0045-7930. DOI: [http://dx.doi.org/10.1016/0045-7930\(94\)00032-T](http://dx.doi.org/10.1016/0045-7930(94)00032-T). URL: <http://www.sciencedirect.com/science/article/pii/004579309400032T>.
- [16] E. Michaelides. Review—the transient equation of motion for particles, bubbles, and droplets. *Journal of fluids engineering* **119.2** (1997), 233–247.
- [17] C. Crowe et al. *Multiphase Flows with Droplets and Particles, Second Edition*. Taylor & Francis, 2011. ISBN: 9781439840504. URL: <http://books.google.se/books?id=XewhTKFFv4EC>.
- [18] C. J. Reagle et al. Measuring the coefficient of restitution of high speed microparticle impacts using a PTV and CFD hybrid technique. *Measurement Science and Technology* **24.10** (2013), 105303. URL: <http://stacks.iop.org/0957-0233/24/i=10/a=105303>.
- [19] U. Ojaniemi et al. Wall function model for particulate fouling applying {XDLVO} theory. *Chemical Engineering Science* **84** (2012), 57–69. ISSN: 0009-2509. DOI: <http://dx.doi.org/10.1016/j.ces.2012.08.004>. URL: <http://www.sciencedirect.com/science/article/pii/S0009250912004927>.
- [20] A. Guha. A generalized mass transfer law unifying various particle transport mechanisms in dilute dispersions. English. *Heat and Mass Transfer* **44.11** (2008), 1289–1303. ISSN: 0947-7411. DOI: 10.1007/s00231-008-0369-5. URL: <http://dx.doi.org/10.1007/s00231-008-0369-5>.
- [21] P. Gullberg and L. Löfdahl. “An Investigation and Correction Method of Stationary Fan CFD MRF Simulations”. *Thermal System Efficiencies Summit*. 2009.
- [22] E. Ljungskog and U. Nilsson. “CFD for Underhood Modeling. Development of an Efficient Method”. MA thesis. Chalmers University of Technology, 2014.
- [23] P. Gullberg and L. Löfdahl. “A Correction Method for Stationary Fan CFD MRF Models”. *SAE World Congress & Exhibition*. 2009.
- [24] P. Gullberg et al. *Continued Study of the Error and Consistency of Fan CFD MRF Models*. Tech. rep. SAE Technical Paper, 2010.

- [25] N. E. Ahmad, E. F. Abo-Serie, and A. Gaylard. Mesh optimization for ground vehicle aerodynamics. *CFD Letters* **2.1** (2010), 54–65.
- [26] K. Okumura. *CFD simulation by automatically generated tetrahedral and prismatic cells for engine intake duct and coolant flow in three days*. Tech. rep. SAE Technical Paper, 2000.

A Appendix

A.1 The influence of rotation of particles

A test was performed to analyze the influence of rotation on particles. The test was performed by using the Discrete Element Method (DEM) mode in STAR-CCM+. In the DEM mode the linear spring collision model can be added while in the lagrangian mode. The set up shown in Table A.1 and A.2 is very similar except for the use of DEM particles and DEM mode.

Table A.1: Models for the air in STAR-CCM+.

| DEM mode | Lagranian unsteady model | Lagrangian steady model |
|---------------------------------|---------------------------------|---------------------------------|
| Coupled Energy | Coupled Energy | Coupled Energy |
| Coupled Flow | Coupled Flow | Coupled Flow |
| Discrete Element Model (DEM) | | |
| Implicit Unsteady | Implicit Unsteady | Steady |
| Gas | Gas | Gas |
| Gradients | Gradients | Gradients |
| Ideal Gas | Ideal Gas | Ideal Gas |
| K-Epsilon Turbulence | K-Epsilon Turbulence | K-Epsilon Turbulence |
| Lagrangian Multiphase | Lagrangian Multiphase | Lagrangian Multiphase |
| Realizable K-Epsilon Two-Layer | Realizable K-Epsilon Two-Layer | Realizable K-Epsilon Two-Layer |
| Reynolds-Averaged Navier-Stokes | Reynolds-Averaged Navier-Stokes | Reynolds-Averaged Navier-Stokes |
| Three Dimensional | Three Dimensional | Three Dimensional |
| Turbulent | Turbulent | Turbulent |
| Two-Layer All y+ Wall Treatment | Two-Layer All y+ Wall Treatment | Two-Layer All y+ Wall Treatment |

The test was performed in a very small domain shown in Figure A.1 and the particles was 1mm in diameter and was released with a velocity of 3m/s and the fluid was 1m/s in the inlet.

A.2 Results from the rotation of particles

As it can be seen in Figures A.2 and A.3 there is some difference in the behavior of the particles when rotation and more advanced collision models is applied. As can be seen in Figures A.2a and A.2b, the difference when adding time dependency is very low though. The Table A.3 shows that when adding the DEM mode the time factor increases with 5200 times compared to the steady case, while the unsteady increases with 116 times. The time in Table A.3 when using a 4 core Intel Xeon W352@2.67Ghz processor.

Table A.2: Models for the Lagrangian phase in STAR-CCM+.

| DEM mode | Lagranian modes |
|-------------------------|-------------------------|
| Constant Density | Constant Density |
| DEM Particles | Material Particles |
| Drag Force | Drag Force |
| Drag Torque | Material Particles |
| Pressure Gradient Force | Pressure Gradient Force |
| Solid | Solid |
| Spherical Particles | Spherical Particles |
| Track File | Track File |
| Turbulent Dispersion | Turbulent Dispersion |
| Two-Way Coupling | Two-Way Coupling |

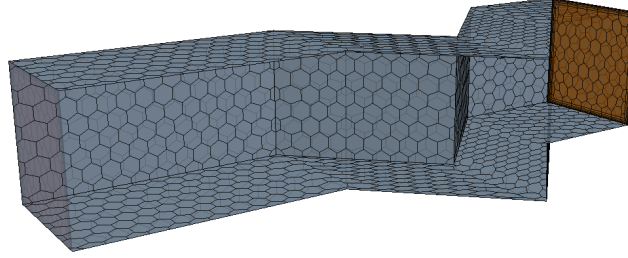
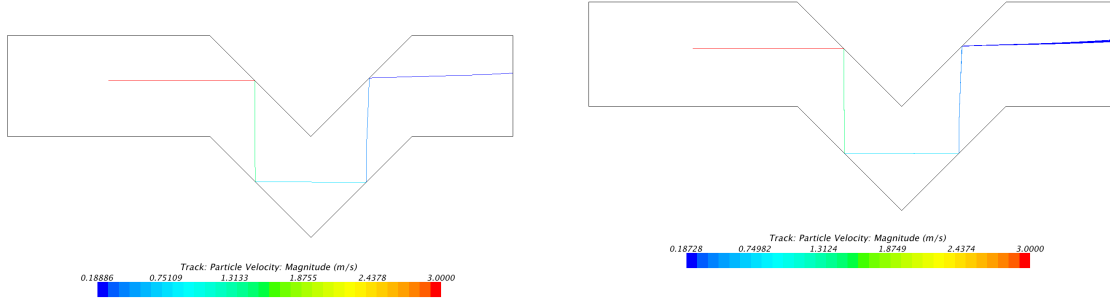
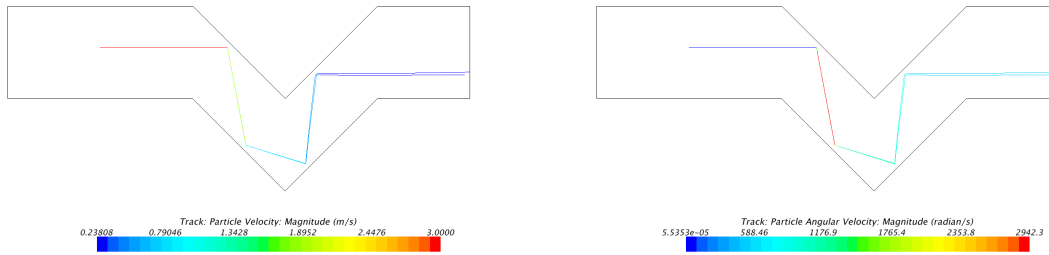


Figure A.1: *The domain for testing rotation of particles.*



(a) *The velocity of the particle for the steady case.* (b) *The velocity of the particle for the unsteady case (note that the plot shows two particles).*

Figure A.2: *The velocity of the particles for the Lagrangian phases.*



(a) *The velocity of the particle* (b) *The angular velocity of the particle*

Figure A.3: *The velocity and angular velocity of the DEM mode case*

Table A.3: The time and time factor for a particle to go through the domain.

| | Time | Time factor |
|--------------------------|---------|-------------|
| DEM mode | 3900sec | 5200 |
| Lagrangian unsteady mode | 87sec | 116 |
| Lagrangian steady mode | 0.75sec | 1 |